Title: Calcium phosphate substrates with emulsion-derived roughness: processing, characterisation and interaction with human mesenchymal stem cells

Authors: Gil Costa Machado, Esther García-Tuñón, Robert V. Bell, Mauro Alini, Eduardo Saiz, Marianna Peroglio

PII: S0955-2219(17)30466-1
DOI: http://dx.doi.org/doi:10.1016/j.jeurceramsoc.2017.06.043
Reference: JECS 11347

To appear in: *Journal of the European Ceramic Society*

Received date: 15-2-2017
Revised date: 7-6-2017
Accepted date: 24-6-2017

Please cite this article as: Machado Gil Costa, García-Tuñón Esther, Bell Robert V, Alini Mauro, Saiz Eduardo, Peroglio Marianna.Calcium phosphate substrates with emulsion-derived roughness: processing, characterisation and interaction with human mesenchymal stem cells.*Journal of The European Ceramic Society* http://dx.doi.org/10.1016/j.jeurceramsoc.2017.06.043

Calcium phosphate substrates with emulsion-derived roughness: processing, characterisation and interaction with human mesenchymal stem cells

Gil Costa Machado[1], Esther García-Tuñón[2,3], Robert V. Bell[4], Mauro Alini[5], Eduardo Saiz[1], Marianna Peroglio[5]

[1]Department of Materials, Imperial College London, South Kensington, London, SW7 2BP, UK
[2]Materials Innovation Factory, University of Liverpool
[3]School of Engineering, University of Liverpool
[4]Department of Chemistry, University of Warwick, Coventry, CV4 7AL, UK
[5]AO Research Institute Davos, Switzerland

Corresponding author
g.machado@imperial.ac.uk (Gil Costa Machado)
New e-mail: g.machado@manchester.ac.uk

ABSTRACT

Calcium phosphates (CaP) have been the subject of several studies that often lack a systematic approach to understanding how their properties affect biological response. CaP particles functionalised with a pH-responsive polymer (BCS) were used to prepare microporous substrates (porosity between 70-75% and pore sizes of 5-20μm) through the aggregation of oil-in-water emulsions by controlling solid loading, emulsification energy, pH, drying and sintering conditions. The combined effect of surface roughness (roughness amplitude, R_a between 0.9-1.7μm) and chemistry (varying Hydroxyapatite/β-Tricalcium phosphate ratio) on human mesenchymal stem cells was evaluated. HA substrates stimulated higher cell adhesion and proliferation (especially with lower R_a), but cell area increased with β-TCP content. The effect of surface roughness depended of chemistry: HA promoted higher mineralising activity when R_a~1.5μm, whereas β-TCP substrates stimulated a more osteogenic profile when R_a~1.7μm. A novel templating method to fabricate microporous CaP substrates was developed, opening possibilities for bone substitutes with controlled features.

Keywords: Calcium phosphates; Emulsions; Microporosity; Surface roughness; human mesenchymal stem cells

1. INTRODUCTION

Millions of people suffer bone injuries every year, either accidental or disease related, that call for the use of bone substitutes with controlled properties to promote cell migration, adhesion, differentiation and ultimately formation of new bone. All this, while they degrade

at a controlled rate and stimulate vascularisation of the injury site. Chemical composition, macroporosity (> 100 μm) and pore interconnectivity are all known to be essential for the final outcome of a bone graft *in vivo* [1]. However, a few studies have addressed the possibility that microporosity in the range of 0.1 to 10-20 μm, i.e. at the cellular level, may play a crucial role on the formulation of cell response, possibly increasing material bioactivity [2]. Furthermore, these features could also prove advantageous in chemical delivery strategies, in which micropores can act as "drug reservoirs". Integrating features at this scale in large scaffolds with complex shape, while maintaining control of macropores and chemistry, remains a significant challenge.

Emulsions – the mixture of two immiscible liquids, where one is dispersed as drops in the continuous phase of the other - have a wide range of applications in the food, cosmetic and pharmaceutical industries [3] as well as in processing. The stabilisation of the interface is key for emulsification and long-term stability. This can be provided by different approaches, either by using a surfactant or fine solid particles that tend to segregate at the interface [4]. The latter, known as particle stabilised emulsions or Pickering emulsions [5], are currently used in different ceramic processing technologies [6]. Recent advances demand greater functional control from them, such as the ability to control the rheology for extrusion [7] or to respond to external stimuli [8]. Different stimuli such as temperature [3], CO_2 [8], magnetic fields [9], salt concentration [10] and light intensity [11] have been used. pH is another very commonly used external trigger. A particle is referred to as pH-responsive when its surface charge is altered by changes in proton concentration in the environment, which then changes how the material interacts with its surroundings [12]. Whether non-modified particles (organic or inorganic) or surface functionalised particles (both covalently and non-covalently) are used, simply tuning the pH of the system causes protonation or deprotonation of pH-responsive functional groups, changing the behaviour of the particle surface and consequently, altering the stability of the emulsion. An example of particle surface functionalisation is that obtained with a pH-responsive branched copolymer surfactant (BCS) [13], which has been previously used to functionalise the surface of ceramic materials to control their processability [14]. The BCS is a copolymer made of branches with different functionalities: methacrylic acid (MAA), poly(ethyleneglycol) methacrylate (PEGMA), ethyleneglycol dimethacrylate (EGDMA) and 1-dodecanethiol (DDT). EGDMA functionalities allow the crosslinking of polymer chains during BCS preparation, creating its branched character. DDT chain ends are used to provide hydrophobicity, making it an amphiphilic molecule. Overall, the branched architecture of the BCS ensures that multiple

potential points of attachment to both water-oil interfaces and ceramic particles in suspension are available [15]. Most systems that use emulsions as structural templates for porous calcium phosphates are concerned with the fabrication of hydroxyapatite microspheres [16-18] and nanoparticles [19]. The feasibility of emulsions containing α-TCP and HA in the aqueous phase [20], as well as β-TCP [21], has also been reported. A more recent study where pH-responsive calcium phosphate particles and fibres were used to make porous materials has been performed, but with poor structural results [22].

Several studies have tried to understand the combined effect of structural features and chemical composition of calcium phosphates on bone cell behaviour, with no clear consensus being achieved [2]. For example, cell attachment and adhesion have been shown to increase when roughness increases [23]. The effect on cell proliferation is less clear, as the same study showed osteoblasts proliferate more on HA substrates with increasing roughness, while other study found that human osteoblasts proliferate less on rougher calcium phosphate substrates [24]. Common methods of tailoring microstructural features of calcium phosphates include varying sintering conditions (to obtain intergranular porosity) [25, 26] and polishing surfaces to study the effect of roughness on cell behaviour [23, 27], but these methods are either difficult to reproduce or not translatable into 3D scaffolds. Precipitation of biomimetic HA coatings from saturated solutions has also been used to prepare surfaces with varying roughness [28]. More recent approaches use porogens (e.g. polymethylmethacrylate [29-34] or wax granules [35]) as sacrificial templates to make micropores (2-8 μm) in the bulk material, in combination with other casting techniques, such as robocasting, to produce large pieces capable of filling a bone defect and conduct bone ingrowth. These present limitations in the range of pore sizes and interconnectivity obtained, as well as requiring further thermal treatments to eliminate PMMA particles [30], posing an additional burden on the microstructure. Calcium phosphates with varying composition – usually ranging from pure HA to pure β-TCP, including biphasic compositions – have been investigated for their effect on bone cell response. Bioactivity is related to the dissolution behaviour of the ceramic, which can be controlled by changing the chemical composition, among other properties [36]. In this sense, one would expect TCP-based materials to be more bioactive than HA-based materials due to their increased solubility at physiological conditions [37]. However, some studies have found HA substrates often promote higher ALP activity in human osteoblasts [24, 38].

In this study, ceramic substrates were prepared by functionalising CaP powders with BCS to make cellular solids through an emulsification process, thus obtaining great control of their microstructure independently of the chemistry. A framework was designed to understand the combined effect of chemistry and microporosity (1-10 μm) of two-dimensional calcium phosphate substrates with varying HA/β-TCP ratio on the behaviour of hMSCs *in vitro*.

2. MATERIALS AND METHODS

2.1. Preparation of BCS aqueous solutions at pH=8

pH-responsive BCS with a composition of PEGMA5-MAA95-EGDMA10-DDT10 was synthesised as described elsewhere [13]. Aqueous solutions with various concentrations were prepared: 0.5-8 wt%. BCS was added to distilled water under stirring at room temperature and the pH was adjusted to 8 with 1M NaOH.

2.1.2. Functionalisation of calcium phosphate particles with BCS

Hydroxyapatite and β-Tricalcium phosphate powders (Keramat, Spain) were used. HA had an average crystal size of 200 nm and a surface area of 9.68 m^2/g. β-TCP presented an average crystal size of 0.5-1 μm and a surface area of 3.87 m^2/g. Powders with varying HA/β-TCP wt% were suspended in a BCS aqueous solution (pH=8) in a range of solid loadings (10-70 wt/v%) and mixed in a bench top ball-miller (low speed, 48h). Density values of 3.15 g/cm^3 [39] and 3.07 g/cm^3 [40] were used for HA and β-TCP, respectively. Average particle diameter was evaluated on 10 wt/v% suspensions with a Malvern Mastersizer Hydro 2000SM. Suspensions with up to 70 wt% (with respect to water) were prepared. Dolapix CA (Aschimmer & Schwarz GmbH & Co) was used to disperse ceramic particles in aqueous suspensions for comparison.

2.2. Emulsification of BCS-functionalised ceramic suspensions, aggregation and drying

Emulsions were prepared by adding an equal volume (50 vol% of the final emulsion) of decane ($CH_3(CH_2)_8CH_3$, Sigma-Aldrich) to the BCS-functionalised ceramic suspension. After a 2-3 second step of manual shaking, an additional step of mechanical high-energy stirring was performed at 24000 rpm (IKA S 25 -10 G Dispersing tool connected to an IKA ULTRA-TURAX homogenizer) for 1-10 minutes. Glucono-δ-lactone (GδL, ≥99%, Sigma Aldrich) was added to the materials by gently stirring with a spatula to drop the pH. The materials

were poured into moulds (greased with vaseline) and allowed 24 hours at room temperature to aggregate. After that, samples were dried for 3-4 days at 37°C.

2.3. Fluorescence microscopy

The branched BCS architecture was modified with rhodamine for fluorescence. Emulsified suspensions (10 wt/v% HA) containing rhodamine modified BCS (BCSr) were imaged with a Zeiss Axio Scope.A1 optical microscope, using an immersion 100x ocular (N-Achroplan 100x/1.25 Oil iris WD0.29M27), fluorescence-free immersion oil and rhodamine fluorescence filter (FL Filter Set 43 CY 3 Shift free).

2.4. Thermal treatment of BCS-functionalised materials

All materials underwent the following thermal treatment: slow heating (1°C/min) up to 500°C, with a 2 hour dwell; a faster heating step (5°C/min) was used to reach the sintering temperature (1h dwell), which varied with the initial HA/β-TCP ratio: 1120°C for pure HA, 995°C for pure β-TCP and 1140°C, 1105°C and 1090°C for biphasic compositions 75/25, 50/50 and 27/75 wt% (HA/TCP), respectively. Samples were allowed to cool to room temperature.

2.5. Porosity and mechanical characterisation

The porosity of the ceramic materials was determined by the Archimedes method and their microstructure was studied with Scanning Electron Microscopy (LEO Gemini 1525) images of fracture surfaces. The compressive strength of 5x5x5 mm^3 calcium phosphate porous materials (n=10) was measured in a universal mechanical testing machine (model Z010, Zwick Roell, Germany), following the ASTM C133-94 standard at 1.3 mm min^{-1}. Specimens were cut from a ceramic part with a diamond blade and grinded to ensure parallel surfaces. In order to homogeneously distribute the load, a stainless steel hemisphere was placed on top of the samples.

2.6. Substrates for *in vitro* cell cultures

'No oil' substrates were prepared using three compositions (pure HA, HA/β-TCP 50/50 wt%, pure β-TCP) with a solid loading of 70 wt% and functionalised in BCS 2 wt%. For each composition, samples with three different microstructures were obtained: 1) "No oil",

prepared from ceramic suspensions to which no decane was added; 2) “2.5 min”, prepared from ceramic suspensions to which 50 vol% of decane was added and stirred for 2.5 minutes; 3) “1 min”, prepared from ceramic suspensions to which 50 vol% of decane was added and stirred for 1 minute. After aggregation (1 wt/v% GδL), drying and sintering, 2mm thick discs were cut with a diamond blade (Buehler IsoMet Wafering Blade 15LC) at low speed. Samples were polished with 1200 grit SiC and washed in a sonicator with deionised water and successive washes in ethanol. Finally, the discs were sterilised by dry heat at 180°C for 5 hours.

2.7. Surface analysis of ceramic substrates

Ceramic discs with three different surface types (no oil, 2.5 min and 1 min) were coated with a 30 nm Au layer and their roughness was measured with a Zygo light interferometer. MetroPro software (version 9.1.1) was used to analyse the results and obtain average roughness amplitude values (n=5).

2.8. Human mesenchymal stem cell expansion and seeding

Human mesenchymal stem cells (hMSCs) were isolated from human bone marrow aspirates obtained from the University Hospital of Bern after approval by the local ethical commission (KEK 188/10) and written consent of the patient. Bone marrow was shipped at room temperature from Bern to Davos and hMSCs were isolated by Ficoll gradient centrifugation and adherence to tissue culture plastic. Cell expansion was performed in α-minimum essential medium (α-MEM) containing penicillin (100 U/mL) and streptomycin sulfate (100 µg/mL) (Gibco, Basel, Switzerland), 10% foetal bovine serum (Sera Plus, Pan-Biotech, Aindenbach, Germany) and 5 ng/mL basic fibroblast growth factor (R&D Systems, Minneapolis, MN, USA) with a medium change twice a week. Early passage (P2–P4) hMSCs from three different donors were used.

hMSCs were seeded on the surface of the samples at a density of 10000 cells/cm^2. Samples were cultured in osteogenic medium, composed of Dulbecco's modified essential medium (DMEM) containing 4.5 g/L glucose, penicillin (100 U/mL) and streptomycin sulfate (100 µg/mL) (Gibco, Basel, Switzerland), 10% foetal calf serum (Sera Plus, Pan-Biotech, Aindenbach, Germany), 50 µg/mL ascorbic acid (Sigma-Aldrich, Buchs, Switzerland, cat.n. A8960), 5 mM β-glycerophosphate disodium salt hydrate (Sigma-Aldrich) and 100 nM dexamethasone (Sigma-Aldrich). Samples were cultured in 24-well places with 1

mL medium/well and medium changes three times a week. Thermanox® coverslips (13 mm diameter, Thermo Fisher Scientific, Reinach, Switzerland) were used as controls.

Experiments were conducted with hMSCs from three different donors. In each experiment, triplicates of the samples were used for each type of analysis and time point. Blanks (materials without cells) were measured and were <10% of the value of the samples.

2.9. Cell morphology

Cell morphology was characterised after 2 and 48 hours of incubation on ceramic substrates in osteogenic medium. First, samples were washed in PBS and fixed in 0.5mL of 0.1M PIPES (1,4-piperazinediethanesulfonic acid) at pH 7.4 for 2 min. Then cells were incubated in 250µL of 2.5% glutaraldehyde in 0.1M PIPES for 5 min, and rinsed again in 0.5mL of 0.1M PIPES for 2 minutes. Post-fixation was performed with 1% osmium tetroxide (Simec Trade AG, Switzerland) in 0.1M PIPES (pH 6.8) for 1 hour (protected from light). Samples were rinsed with 1mL deionised water for 2 min (3 times), cells were dehydrated in successive ethanol solutions (50, 60, 70, 80, 90, 96, 100%) for 5 minutes each and critical point dried in a POLARON E300 (Agar Scientific, UK) [41]. Cells were coated with a 10 nm layer of Au/Pd (Baltec MED020, Bal-Tec Liechtenstein) and imaged in a S-4700 Field Emission Scanning Electron Microscope (Hitachi, Japan) at a WD of 13 mm (5 kV, 40 µA). SEM images were quantitatively analysed using ImageJ software (1.48v). Cell area and perimeter were determined by manual contour of cells from different images and duplicates (n>40), with the exception of two conditions where cell adhesion was lower (HA “No oil” 48h and BCP “No oil” 48h).

2.10. DNA content

Cell attachment and proliferation were assessed by quantifying the DNA content with Quant-iT PicoGreen cell proliferation assay (Invitrogen, Basel, Switzerland). At day 1, 7, 14, 21 and 28 of culture, samples were rinsed with phosphate buffered saline (PBS) (pH=7.4) and cells were lysed with 500 µL of 0.1% Triton-X in 10 mM Tris-HCl (pH=7.4) (both from Sigma-Aldrich) for 2 hours at 4°C on a shaker and lysates were stored at -80°C. The assay was performed according to the manufacturer instructions with λ-DNA as standard. Fluorescence of each sample was measured with 485 nm excitation and 530 nm emission filters on a plate reader (Victor 3, Perkin Elmer, Wellesley, MA, USA).

2.11. Alkaline phosphatase activity and staining

Alkaline phosphatase (ALP) activity was measured on the same cell lysates used for DNA quantification, as described by Tirkkonen [42]. After 15 min incubation at 37°C with p-nitrophenyl phosphate as substrate (Sigma Kit No.104), the absorbance was measured at 405 nm following an incubation time of 15 minutes. The enzyme activity was expressed as µmoles of p-nitrophenol liberated per minute and normalised to the DNA content of each sample. At specific time points (day 7, 14, 21 and 28) cells were rinsed with PBS and stained using a leukocyte alkaline phosphatase kit (Sigma-Aldrich, cat.n. 85L3R-1KT) according the manufacturer instructions. Overview images were obtained with a MacroFluo (Leica). The pixelsize was 15.2 µm.

2.12. RNA isolation, complementary DNA preparation and quantitative real-time polymerase chain reaction

Total RNA was extracted with 500 µl TRI reagent (Molecular Research Center, Cincinnati, OH, USA) and 2.5 µl polyacrylamide carrier (Molecular Research Center) according to the manufacturer instructions. Complementary DNA was obtained by reverse transcription of 200 ng of total RNA, using TaqMan reverse transcription reagents (Applied Biosystems, Foster City, CA) with random hexamer primers on a Thermal Cycler 9600 (Applied Biosystems, Rotkreuz, Switzerland). Real-time Polymerase Chain Reaction (PCR) was performed on a QuantStudio 6 Flex (Applied Biosystems, Foster City, CA). Genes of interest were detected using specific oligonucleotide primers and TaqMan probes (Microsynth, Balgash, Switzerland) or Assays on Demand (Applied Biosystems) (Table 1), using TaqMan Universal PCR master mix (Applied Biosystems). Quantification of mRNA targets was performed according to the comparative C_T method with 18S ribosomal RNA as endogenous control. hMSCs at seeding time were used for relative comparison.

2.13. Statistical analysis

After testing the normal distribution of the measurements, data were compared using a two-way ANOVA test with Dunnett's correction. Differences were considered as significant when $p < 0.05$ (*), $p < 0.01$ (**), $p < 0.001$ (***) and , $p < 0.0001$ (****). a ($p < 0.05$), b ($p < 0.01$), c ($p < 0.001$) and d ($p < 0.0001$) refer to differences between Control and ceramic substrate at the same time point. * refers to the same group at different time points. # refers to differences between different chemical compositions, but same surface type.

3. RESULTS

3.1. CaP particle functionalisation with BCS

From DLS measurements (Fig. 2A), BCS-functionalised HA has a monodisperse distribution and seems to be better dispersed when using a BCS concentration of 4 wt% (D_{50} = 3.169 ± 0.048 μm), with a small variation in the range 1-4 wt%. In the case of β-TCP (Fig. 2B), agglomerates are formed when higher BCS concentrations (4 and 8 wt%) are used, and the best dispersion is obtained for BCS concentrations between 1 and 2 wt%. Therefore, 2 wt% of BCS was chosen as an adequate concentration for both materials. Suspensions dispersed with Dolapix present the highest average particle size (4.103 ± 0.004 μm). Figure 2C demonstrates how BCS 2 wt% disperses and stabilises the ceramic materials in a similar way to Dolapix.

The effect of GδL - used to lower the pH and promote the aggregation of ceramic suspensions - was evaluated in two conditions: BCS in water solutions (Fig. 2D); and BCS aqueous solutions with ceramic particles (Fig. 2E). The pH of BCS 2 wt% solutions in water (Plot D), followed for 24 hours, decreased faster and to a greater extent for higher amounts of GδL. Considering the initial pH (before GδL addition) of the BCS solution was 8, it becomes clear that a sharp pH reduction occurred in the first minutes. Plus, the solution with 4 wt/v% GδL became opaque between 2 and 4 hours, 5.06 > pH > 4.38 (area in blue). The same occurred with the 2 wt/v% GδL solution after 12 hours. Hence, 1 wt/v% GδL was the standard concentration used. Plot E shows that, before the addition of GδL (time = 0 min), higher solid content lead to a slightly higher pH for both HA and TCP. After GδL addition, in the 24h of pH stabilisation, suspensions made with TCP suffered a larger pH decrease (pH<6) than HA. Overall, the pH of ceramic suspensions is lower than that of the BCS 2 wt% solution with no particles (thick line). In the case of emulsions (dashed lines), pH decreases more slowly in the first minutes, but it eventually reaches the values of the correspondent ceramic suspension, being identical after 24 hours. Therefore, a period of 24 hours was considered enough for pH to reach a stable value in the preparation of ceramic scaffolds.

3.2. Interface stabilisation

Figure 3A-C shows how BCSr (rhodamine modified BCS) performs in low solid content emulsions before GδL-triggered aggregation. With the oil droplets in the same plane of depth, it is possible to observe how the system promotes the tight packing of the oil

droplets. At first, one can observe the continuous phase, i.e., where the fluorescent BCSr-functionalised HA particles are. Focusing on the plane that crosses the oil droplets, only a thin layer separates adjacent oil droplets and no droplet coalescence is observed. Going further down, the volume of the continuous phase is observed again, with the appearance of some smaller droplets between the larger ones. Individual BCS-functionalised particles – of the same size as indicated by the DLS measurements – are evidenced by a local increase in fluorescence, and can be seen through large oil droplets (Fig. 3B). Fig. 3C shows a local increase of BCSr at the interface between the oil droplets and the continuous phase.

3.3. Solid content

Fig. 3D shows representative SEM images of microporous HA and β-TCP materials prepared with solid content of 60-70 wt%. Top row presents images of green bodies, held together by the BCS adsorbed to the particles, where the micropores left after oil evaporation are discernible. The 70 wt% sintered constructs present the final microstructure that resembles the organisation seen in the fluorescence microscopy images more closely. The porosity is highly interconnected, with openings between adjacent pores where a layer of BCS prevented two oil droplets from coalescing. Reducing the solid content (60 wt%), the structure provided by the oil droplets is still visible. However, walls have occasional defects. By lowering the solid loading to 45 wt% (not shown), the microstructural organisation is severely compromised and the integrity of the sample deteriorates during drying and sintering. Overall, the structures are more self-supporting when prepared with higher solid loading and their organisation is similar for HA and TCP.

3.4. Emulsification energy

After the manual agitation step, during which the o/w emulsion was formed, further oil droplet breakdown was obtained with a stirrer for different periods (1, 2.5 and 10 minutes) with no temperature increase detected. Figure 4A shows the evolution of the microstructure of HA and β-TCP constructs emulsified with increasing energy. The average pore size in the final materials decreases when more energy is introduced into the mixture of ceramic suspension and decane (Fig. 4B). After manual agitation, the average pore size is around 20 μm for both materials, with a wide distribution. When stirring mechanically, droplet breakdown occurs quickly. The average pore size of emulsions stirred for 2.5 minutes (4.19 ± 1.42 μm for HA, 4.67 ± 2.12 μm for β-TCP) is only slightly higher than that of structures emulsified for 10 minutes (3.83 ± 1.75 μm for HA, 4.22 ± 2.01 μm for β-TCP). A

significantly higher average pore size is obtained when stirring only for 1 minute: 7.18 ± 1.61 μm for HA and 7.32 ± 1.97 μm for β-TCP). Total porosity of the ceramic constructs is constant (72-74%) for all conditions, with closed porosity in the range 4-7%. Linear shrinkage of HA and β-TCP (before β→α transformation) during sintering was of 12% and 11%, respectively, with chemistry thus not having a significant effect in porosity. Furthermore, compressive strength of the materials decreases with decreasing pore size, an effect more evident in HA materials (Fig. 4C).

3.5. Aggregation, drying and sintering

Among the GδL concentrations studied (0.1, 0.5, 1, 2 and 4 wt/v%), materials aggregated with 0.1-0.5 wt/v% GδL were not able to keep their shape after 3-4 days of drying and their structure collapsed. Higher GδL amounts (1 to 4 wt/v%) provided fast (less than 24 hours) aggregation with complete preservation of external shape and volume. Therefore, 1 wt/v% GδL was the best compromise between the necessary stiffening of the materials, while not reducing the pH too much (possibly causing the dissolution of calcium phosphate). After the 24 hours aggregation period, ceramic constructs were placed in a convection oven at 37°C for up to 4 days, rendering pieces with no cracks or other visible defects. Sintering follows at specific temperatures depending on chemical composition. Fig. 4D shows the microstructure of No oil HA samples. The SEM images show necking between grains, with residual inter-grain porosity. The sintering conditions provide good construct consolidation without compromising porosity and the microstructural features that result from the decane droplets. Plus, phase composition is not altered by the processing and final thermal treatment.

3.6. Discs for *in vitro* cell cultures

Figure 5A presents the surface maps and representative roughness profiles of the three different surface types. First, the samples fabricated without emulsification (No oil) are smoother than the two emulsified materials, where round pits are observed. The correspondent surface line profiles show the No oil samples have a narrower range between peaks and pits (R_a = 0.923 ± 0.064 μm), as well as a narrow distribution of feature size. When comparing the two surfaces resulting from emulsions, the surface of the material prepared with the shortest emulsification time (1 min, R_a = 1.691 ± 0.071 μm) shows both a higher amplitude and wider spacing between features. The substrates emulsified for 2.5 min (R_a = 1.475 ± 0.035 μm) show slightly lower amplitude difference between pits and peaks and

narrower features. The R_a values of the three surface types studied are significantly different from each other and very reproducible (Fig. 5B). SEM images C and D show the microstructure of biphasic materials (50/50 HA/β-TCP wt%). The shape and dimensions of pores are very similar to those obtained in single-phase materials.

3.7. hMSCs culture on CaP substrates in osteogenic medium

3.7.1. Cell morphology

Figure 6 shows representative SEM images of hMSCs cultured for 48h on surfaces with varying chemistry and microstructure. After 2 hours (not shown), cell populations on all materials present varied phenotypes with small and round cells. After 48 hours, differences can be detected in the morphology of hMSCs. Cells seeded on substrates with no microporosity (No oil) are larger and present a more elongated phenotype than those cultured on rougher substrates, independently of chemical composition. Cells cultured on HA 2.5 min materials are a good example of how the surface features that result from the emulsion templating promote the formation of pseudopodia. These results are supported by the quantitative analysis of SEM images (overviews) of all conditions, which provided information about cell area and perimeter (Fig. 6B-C). After 2h, cell populations are very similar and have not had time to spread and/or elongate yet. However, after 48h, the area of hMSCs cultured on No oil substrates increases considerably, with a notable effect of chemistry: cell area increases with increasing β-TCP content in the materials composition. The fact that the effect of chemistry on cell area and perimeter depends on surface microstructure means there is interaction between the two factors, as demonstrated by the two-way ANOVA analysis of interaction with $p<0.0001$. Cell perimeter on No oil substrates is also higher than on rougher ones.

Calcium phosphate substrates cultured up to day 7 were also analysed (Fig. 7). No changes to the surface organisation were observed in that period on β-TCP or HA samples, with either microstructure type. In particular, no differences are observed between samples incubated for 2 and 7 days in osteogenic DMEM, suggesting no apatite layer precipitates in this experiment.

3.7.2. hMSC attachment, proliferation and alkaline phosphatase activity

Cell attachment (Fig. 8A) was measured 24 hours after seeding. hMSCs of all donors attached significantly more to the Control (Thermanox®) than to any of the calcium phosphate materials. Throughout the 28 days incubation period (Fig. 8B), the calcium phosphate substrates promoted significant cell proliferation – often more than in Control. Within each composition, the substrates without oil-derived microporosity promoted higher cell proliferation (the other two donors presented a similar trend). A combined effect of chemistry and topography was observed. Comparing the microporous samples, cell proliferation on HA is higher on substrates with smaller R_a (2.5 min), whereas on β-TCP it is higher on substrates with higher R_a (1 min). There is no significant difference in the case of the biphasic composition.

Figure 9A shows how ALP activity peaks at Day 21 for the materials with No oil microporosity, while no peak was observed on the emulsified materials, independently of the composition. Considering only the microporous substrates, a similar trend to that verified in cell proliferation is observed. On HA, ALP activity was higher for substrates with smaller porosity (i.e. emulsified for 2.5 min), while an opposite trend was observed for TCP. The ALP staining (Fig. 9B) supports this trend. Cells grown on substrates with the lowest R_a (No oil) consistently show earlier and higher mineralising activity than the rougher substrates with similar composition. As to the other two experiments, cells from one donor behaved in a similar fashion, while cells from a third donor presented limited ALP activity.

3.7.3. hMSC gene expression profile

Osteogenic differentiation of hMSCs was evaluated using early (Col1, Runx2), intermediate (ALP) and late (OC) genetic markers. Additionally, the ratio between the transcription factors Runx2/Sox9 was calculated as an indicator of *in vitro* osteogenic potential [43]. Expression of Col I (Fig. 10A) decreases throughout the experiment for Control and all conditions, with no particular trends being detected with chemistry and/or surface properties. ALP expression (Fig. 10B) also peaks early (day 7-14) for Control and No oil HA and β-TCP substrates. However, some emulsified substrates appear to promote later

ALP peaks (day 21-28). As to OC (Fig. 10C), cells seeded on calcium phosphate materials tend to express lower levels with time. The only exception is β-TCP 1 min substrates, where OC expression is highest after 28 days, similarly to Control.

Runx2 (Fig. 11A) and Sox9 (Fig. 11B) expression is generally lower on ceramic substrates than on Control. However, β-TCP materials (especially No oil) promote an increased Runx2/Sox9 ratio (Fig. 11C) up to Day 28.

4. DISCUSSION

A system to fabricate microporous calcium phosphate substrates using particles functionalised with a branched copolymer surfactant and emulsified was presented. The interplay between variables like BCS concentration, solid loading, emulsification and pH (controlled by GδL addition) determines the properties of the ceramic slurry and, consequently, those of the final ceramic construct. The BCS, which adsorbs to the surface of particles enables the control of the attraction/repulsion balance between them, allowing the preparation of ceramic suspensions with very high solid loading (up to 70 wt% HA or β-TCP at pH 8). BCS functionalisation presented the best results at 2 wt% in water (pH=8), with D_{50} around 3.5 μm and 1.6 μm for HA and β-TCP, respectively (Fig. 2C). These are considerably higher than the average crystal sizes (200 nm for HA and 0.5-1 μm for β-TCP particles), which means agglomerates are still formed in these conditions. Higher BCS amounts lead to the formation of large agglomerates (around 100 μm), as shown in light scattering measurements (Fig. 2B), likely due to flocculation.

GδL was shown to have an effect on 2 wt% BCS solutions (no particles, Fig. 2D) proportional to its concentration, similarly to previous work [15]. When 2-4 wt/v% GδL was used, BCS solutions reached pH<5, a range where the solubility of calcium phosphates (especially β-TCP) is very high [37, 44-46], which could compromise initial chemical composition. Plus, polymer gelation occurred, a phenomenon previously described [13]. Therefore, 1 wt/v% GδL was chosen as standard concentration to promote aggregation of ceramic suspensions and emulsions. Indeed, Fig. 2E confirmed that this GδL concentration lowers pH to a range that does not compromise chemical compositions (pH~6), with β-TCP suspensions reaching slightly lower values. In the first 20 minutes, pH in the emulsions

decreases more slowly, suggesting that the presence of the dispersed oil droplets somehow slows down GδL dissolution and hydrolysis. However, after 24h, the pH of emulsions is very similar to that of the correspondent ceramic suspension (no oil) with the same composition.

β-TCP particles increase the pH of the system more than HA powders before adding GδL (Fig. 2E) and, in both cases, higher solid loading leads to a larger increase. Several authors have tried to understand how calcium phosphates behave at different pH. In particular, different values for the isoelectric point (IEP) of HA have been proposed in the range of 6.5-10.2 [47], 10.2 [48], 8.5 [49], 7.3 [50, 51], 6.6 [52] or 6.2 [53]. This is justified by the complex surface charges of HA, which may vary with the preparation method [54]. Fewer studies have investigated surface charge and effect of pH on TCP, with isoelectric point values around 6 being suggested for a form of apatitic tricalcium phosphate [55]. Because the pH of the suspensions increases above 8 with the addition of ceramic particles, it is possible that we are working above their IEP, where both HA and β-TCP particles present negative surface charges. However, once functionalised with BCS, the polymer provides steric dispersion.

A local increase of ceramic particles, noticeable by the increase in BCSr fluorescence, at the interface between the oil droplets and the continuous (hydrophilic) phase (Fig. 3C) confirms the amphiphilic character of BCS is essential to stabilise the emulsion. Considering the effect of solid loading, pore walls become thinner and have less structural integrity when it decreases (Fig. 3D), following the same trend verified in a previous study where BCS was used to make Al_2O_3 and SiC porous structures [56]. Sturzenegger *et al.* [57] have shown how increasing solid loading has a positive impact in both the probability of particles to hit the oil-water interface (P_{hit}) and on the adsorption rate of particles during emulsification (R_{ad}). In fact, the degree of particle coating of freshly ruptured droplets is greatly determined by R_{ad}. If R_{ad} is below a certain critical value, newly formed oil droplets will not be covered by particles quickly enough, causing droplet coalescence (coalescence controlled domain). If, on the other hand, R_{ad} is equal to or higher than such critical value, the freshly formed interface is covered by particles and oil droplets maintain their size (rupture controlled domain). Higher emulsification energy (through longer emulsification) has a similar effect, by increasing P_{hit}. The fact that (for 70 wt% materials) there is a correlation between oil droplet size (as shown by final pore size of the porous materials) and emulsification energy (Fig. 4B) proves that the mixing takes place in the rupture controlled domain. The average pore size was very similar for all compositions: pure HA, pure β-TCP and the biphasic mixture 50/50 wt% HA/β-TCP (Fig. 4). Porosity was constant over all formulations, with closed porosity of

4-7%. The roughness of the substrates (quantified by the average of height absolute values, R_a) was found to differ significantly and reproducibly between the three processing conditions (Fig. 5). The R_a values that characterise the substrates are within a range that has been shown to affect cell behaviour [58].

This study demonstrates the combined effect of surface microroughness and chemical composition of CaPs on the osteogenic differentiation of hMSCs. After 48 hours, hMSCs grown on No oil substrates are larger than on rough samples with similar composition. This agrees with results by Anselme *et al.*, who showed that human osteoblasts spread more on surfaces with low roughness amplitude than on rough ones [59]. In our study, cell area increases for increasing amounts of β-TCP, similarly to what has been observed by dos Santos *et al.*, who studied the growth of human osteoblasts on dense calcium phosphate substrates [24]. Cells on rougher substrates (with oil-derived microporosity) are small and round, extending pseudopodia that interact with the micropores on the material surface (Fig. 6A). These features are smaller than the cell size, in a range that has been shown to promote the formation of focal adhesions [60-62].

A frequent concern in *in vitro* cell studies with bioceramics and bioactive glasses is that of apatite precipitation, which may affect cell response. In Figure 7, we show that no layer of precipitated apatite is formed between day 2 and day 7 of cell culture on either HA or TCP substrates. Lu *et al.* [63] have shown HA and β-TCP are insoluble in cell culture medium, so all calcium and phosphate ions present originate from the medium formulation. Furthermore, Kim *et al.* [64] have described the mechanism of apatite deposition on synthetic hydroxyapatite in Simulated Body Fluid (SBF). There are two main differences between such mechanism and our study. First, SBF is saturated towards HA due to high Ca^{2+} and HPO_4^{2-} concentrations: 2.5 mM and 1.0 mM, as opposed to 1.8 mM and 0.9 mM in DMEM. Second, a key driver for the precipitation of the amorphous calcium phosphate layer are the negative charges on the surface of synthetic HA at physiological pH, which causes the formation of a Ca-rich layer, followed by a Ca-poor layer and eventually a layer with a Ca/P ratio closer to 1.65. However, the role of serum proteins is not considered, which have been shown to inhibit or slow down CaP precipitation [65]. The combination of these factors, together with the observation that no precipitation occurs until day 7, shows that no apatite precipitation occurs in our study.

Surface roughness at the micrometre scale ($1 < R_a < 2$ μm) reduces cell adhesion, as more cells adhere to substrates without oil-derived microporosity (Fig 8A). A review by

Anselme and Bigerelle [58] states that, in the majority of studies, adhesion of bone cells increases when roughness increases, although other studies suggest otherwise. Chemistry appears to have no significant effect on cell adhesion. Although hMSCs generally grow exponentially for all materials, cell proliferation (Fig. 8B) is affected by early cell adhesion, as total cell number on No oil substrates is higher than on rough surfaces until day 28. hMSCs proliferate more on pure HA substrates (HA > BCP > β-TCP), with a clear correlation to HA content. This has been observed in another study with SaOS-2 cells by Wang *et al.*, although the authors suggest microtopography may have an effect as well [38]. The effect of roughness on bone cells has been widely studied on Ti-based surfaces. An example is the work of Deligianni *et al.* [66], who quantified proliferation of osteoblast-like cells and human bone marrow-derived cells on titanium surfaces with R_a between 0.32-0.87 μm and showed that cell proliferation increases with roughness. In another study, cell proliferation (MC3T3-E1 and human osteoblasts) on Ti surfaces with R_a in the range 0.16-3.4 μm decreased as roughness increased [67]. The obvious difference is in the range of roughness at which these studies evaluated cell behaviour. This is a subject previously discussed by Bigerelle *et al.* [68]. They introduced the concept that surface roughness can be separated in two categories: one concerned with the surface features with which cells establish adhesions and interactions; other, at a larger scale, that takes into account the landscape around cells. When considering topography below the cell scale, cells proliferate more on smooth surfaces. On the other hand, when topography is considered above the cell scale, they proliferate (and adhere) more on rough isotropic surfaces. Analysing our results in the light of this approach, the range of surface features used falls in the smallest category, i.e., surface roughness below cell size. And, in that sense, the fact that the No oil substrates (R_a = 0.923 ± 0.064 μm) promote higher cell adhesion and proliferation than the rougher substrates 2.5 min (R_a = 1.475 ± 0.035 μm) and 1 min (R_a = 1.691 ± 0.071 μm) agrees with the findings of Bigerelle *et al.*

ALP activity, a key indicator of osteogenic behaviour [69], peaks at later time points (day 14-28) for hMSCs cultured on ceramic substrates than on Control, especially on the rough ones (Fig. 9). Considering chemistry alone, HA seems to stimulate higher mineralising activity than materials containing TCP, similarly to previous studies [24, 38]. An important trend concerns the combined effect of chemistry and topography on ALP activity: optimal roughness will vary depending on the surface chemistry. In particular, cells grown on HA have higher ALP activity when cultured on surfaces with lower Ra (2.5 min), while cells

grown on rougher TCP samples (1 min) present higher ALP activity than on those emulsified for 2.5 min. Yuan *et al.* [70] make a comprehensive study of the effect of chemistry (HA, BCP and β-TCP) and microstructure (grain size and density controlled by sintering) on the *in vitro* behaviour of human bone marrow-derived stem cells and on *in vivo* osteoinduction (ectopic implantation in dog muscle tissue). They showed that TCP induced the most osteogenic profile on MSCs *in vitro*, unlike what was observed in our study. Finally, ALP (Fig. 10B) and the Runx2/Sox9 ratio (Fig. 11C) were upregulated when compared to control on most TCP-containing substrates. Overall, HA substrates promoted higher cell attachment, proliferation and mineralising activity, but the effect of chemistry is dependent on surface topography.

5. CONCLUSIONS

This study provided an important insight into the phenomena that control the organisation of emulsions stabilised by BCS-functionalised calcium phosphates. A novel reproducible method to fabricate microporous calcium phosphate substrates was developed, which allows the control of the average pore size (between 3-20 μm) independently of the chemistry used: from pure HA to pure β-TCP, including biphasic compositions. Variables like BCS concentration, solid content, emulsification energy, GδL concentration, drying conditions and final thermal treatment all have an impact in the properties of the calcium phosphate substrates. The study evaluated the osteogenic potential of CaP substrates with controlled microstructural features and chemistry on hMSCs. Overall, thorough characterisation of systems and materials must be performed to allow studies to be compared and trends to be inferred. This study demonstrated that HA substrates stimulate more cell proliferation and mineralising activity when they present a R_a ~1.5 μm, whereas those prepared with β-TCP promote that same behaviour when they have higher roughness (R_a ~1.7 μm), thus suggesting an interdependence of the two variables studied.

6. ACKNOWLEDGEMENTS

The authors would like to acknowledge the European Commission funding under the 7th Framework Programme (Marie Curie Initial Training Networks; grant number: 289958, Bioceramics for bone repair).

REFERENCES

[1] V. Karageorgiou, D. Kaplan, Porosity of 3D biomaterial scaffolds and osteogenesis, Biomaterials 26(27) (2005) 5474-5491.
[2] M. Bohner, Y. Loosli, G. Baroud, D. Lacroix, Commentary: Deciphering the link between architecture and biological response of a bone graft substitute, Acta Biomaterialia 7(2) (2011) 478-484.
[3] B.P. Binks, R. Murakami, S.P. Armes, S. Fujii, Temperature-Induced Inversion of Nanoparticle-Stabilized Emulsions, Angewandte Chemie 117(30) (2005) 4873-4876.
[4] B.P. Binks, Particles as surfactants—similarities and differences, Current Opinion in Colloid & Interface Science 7(1–2) (2002) 21-41.
[5] S.U. Pickering, Cxcvi.—emulsions, Journal of the Chemical Society, Transactions 91 (1907) 2001-2021.
[6] A.R. Studart, U.T. Gonzenbach, I. Akartuna, E. Tervoort, L.J. Gauckler, Materials from foams and emulsions stabilized by colloidal particles, Journal of Materials Chemistry 17(31) (2007) 3283-3289.
[7] C. Minas, D. Carnelli, E. Tervoort, A.R. Studart, 3D Printing of Emulsions and Foams into Hierarchical Porous Ceramics, Advanced Materials (2016).
[8] J. Tang, P.J. Quinlan, K.C. Tam, Stimuli-responsive Pickering emulsions: recent advances and potential applications, Soft matter 11(18) (2015) 3512-3529.
[9] J. Peng, Q. Liu, Z. Xu, J. Masliyah, Synthesis of interfacially active and magnetically responsive nanoparticles for multiphase separation applications, Advanced Functional Materials 22(8) (2012) 1732-1740.
[10] C. Zhao, J. Tan, W. Li, K. Tong, J. Xu, D. Sun, Ca2+ Ion Responsive Pickering Emulsions Stabilized by PSSMA Nanoaggregates, Langmuir 29(47) (2013) 14421-14428.
[11] Z. Chen, L. Zhou, W. Bing, Z. Zhang, Z. Li, J. Ren, X. Qu, Light controlled reversible inversion of nanophosphor-stabilized pickering emulsions for biphasic enantioselective biocatalysis, Journal of the American Chemical Society 136(20) (2014) 7498-7504.
[12] S. Dai, P. Ravi, K.C. Tam, pH-Responsive polymers: synthesis, properties and applications, Soft Matter 4(3) (2008) 435-449.
[13] J.V.M. Weaver, S.P. Rannard, A.I. Cooper, Polymer-Mediated Hierarchical and Reversible Emulsion Droplet Assembly, Angewandte Chemie 121(12) (2009) 2165-2168.
[14] E. García-Tuñón, G.C. Machado, M. Schneider, S. Barg, R.V. Bell, E. Saiz, Complex ceramic architectures by directed assembly of 'responsive' particles, Journal of the European Ceramic Society 37(1) (2017) 199-211.
[15] R.T. Woodward, L. Chen, D.J. Adams, J.V.M. Weaver, Fabrication of large volume, macroscopically defined and responsive engineered emulsions using a homogeneous pH-trigger, Journal of Materials Chemistry 20(25) (2010) 5228-5234.
[16] S. Fujii, M. Okada, H. Sawa, T. Furuzono, Y. Nakamura, Hydroxyapatite Nanoparticles as Particulate Emulsifier: Fabrication of Hydroxyapatite-Coated Biodegradable Microspheres, Langmuir 25(17) (2009) 9759-9766.
[17] X. Liu, M. Okada, H. Maeda, S. Fujii, T. Furuzono, Hydroxyapatite/biodegradable poly(l-lactide–co-ε-caprolactone) composite microparticles as injectable scaffolds by a Pickering emulsion route, Acta Biomaterialia 7(2) (2011) 821-828.
[18] S. Fujii, M. Okada, T. Nishimura, H. Maeda, T. Sugimoto, H. Hamasaki, T. Furuzono, Y. Nakamura, Hydroxyapatite-armored poly(ε-caprolactone) microspheres and hydroxyapatite microcapsules fabricated via a Pickering emulsion route, Journal of Colloid and Interface Science 374(1) (2012) 1-8.

[19] M. Okada, H. Maeda, S. Fujii, Y. Nakamura, T. Furuzono, Formation of Pickering Emulsions Stabilized via Interaction between Nanoparticles Dispersed in Aqueous Phase and Polymer End Groups Dissolved in Oil Phase, Langmuir 28(25) (2012) 9405-9412.
[20] M. Bohner, Calcium phosphate emulsions: possible applications, Key Engineering Materials 192 (2001) 765-768.
[21] M. Bohner, G.H. van Lenthe, S. Grünenfelder, W. Hirsiger, R. Evison, R. Müller, Synthesis and characterization of porous β-tricalcium phosphate blocks, Biomaterials 26(31) (2005) 6099-6105.
[22] S. Fujii, M. Okada, T. Furuzono, Hydroxyapatite nanoparticles as stimulus-responsive particulate emulsifiers and building block for porous materials, Journal of Colloid and Interface Science 315(1) (2007) 287-296.
[23] D.D. Deligianni, N.D. Katsala, P.G. Koutsoukos, Y.F. Missirlis, Effect of surface roughness of hydroxyapatite on human bone marrow cell adhesion, proliferation, differentiation and detachment strength, Biomaterials 22(1) (2000) 87-96.
[24] E.A. dos Santos, M. Farina, G.A. Soares, K. Anselme, Chemical and topographical influence of hydroxyapatite and β-tricalcium phosphate surfaces on human osteoblastic cell behavior, Journal of Biomedical Materials Research Part A 89A(2) (2009) 510-520.
[25] N. Davison, J. Su, H. Yuan, J. van den Beucken, J. de Bruijn, F. Barrère-de Groot, Influence of surface microstructure and chemistry on osteoinduction and osteoclastogenesis by biphasic calcium phosphate discs, Eur Cell Mater 29 (2015) 314-329.
[26] P. Habibovic, H. Yuan, C.M. van der Valk, G. Meijer, C.A. van Blitterswijk, K. de Groot, 3D microenvironment as essential element for osteoinduction by biomaterials, Biomaterials 26(17) (2005) 3565-3575.
[27] W. Yang, W. Han, W. He, J. Li, J. Wang, H. Feng, Y. Qian, Surface topography of hydroxyapatite promotes osteogenic differentiation of human bone marrow mesenchymal stem cells, Materials Science and Engineering: C 60 (2016) 45-53.
[28] D.O. Costa, P.D.H. Prowse, T. Chrones, S.M. Sims, D.W. Hamilton, A.S. Rizkalla, S.J. Dixon, The differential regulation of osteoblast and osteoclast activity by surface topography of hydroxyapatite coatings, Biomaterials 34(30) (2013) 7215-7226.
[29] J. Cesarano, J.G. Dellinger, M.P. Saavedra, D.D. Gill, R.D. Jamison, B.A. Grosser, J.M. Sinn-Hanlon, M.S. Goldwasser, Customization of Load-Bearing Hydroxyapatite Lattice Scaffolds, International Journal of Applied Ceramic Technology 2(3) (2005) 212-220.
[30] J.G. Dellinger, J. Cesarano, R.D. Jamison, Robotic deposition of model hydroxyapatite scaffolds with multiple architectures and multiscale porosity for bone tissue engineering, Journal of Biomedical Materials Research Part A 82A(2) (2007) 383-394.
[31] J.G. Dellinger, A.M. Wojtowicz, R.D. Jamison, Effects of degradation and porosity on the load bearing properties of model hydroxyapatite bone scaffolds, Journal of Biomedical Materials Research Part A 77A(3) (2006) 563-571.
[32] J.G. Dellinger, J.A.C. Eurell, R.D. Jamison, Bone response to 3D periodic hydroxyapatite scaffolds with and without tailored microporosity to deliver bone morphogenetic protein 2, Journal of Biomedical Materials Research Part A 76A(2) (2006) 366-376.
[33] S.K. Lan Levengood, S.J. Polak, M.B. Wheeler, A.J. Maki, S.G. Clark, R.D. Jamison, A.J. Wagoner Johnson, Multiscale osteointegration as a new paradigm for the design of calcium phosphate scaffolds for bone regeneration, Biomaterials 31(13) (2010) 3552-3563.
[34] S.J. Polak, S.K.L. Levengood, M.B. Wheeler, A.J. Maki, S.G. Clark, A.J.W. Johnson, Analysis of the roles of microporosity and BMP-2 on multiple measures of bone regeneration and healing in calcium phosphate scaffolds, Acta Biomaterialia 7(4) (2011) 1760-1771.

[35] J. Zhang, L. Sun, X. Luo, D. Barbieri, J.D. de Bruijn, C.A. van Blitterswijk, L. Moroni, H. Yuan, Cells responding to surface structure of calcium phosphate ceramics for bone regeneration, Journal of Tissue Engineering and Regenerative Medicine (2017) n/a-n/a.
[36] R.Z. LeGeros, Calcium phosphate-based osteoinductive materials, Chemical reviews 108(11) (2008) 4742-4753.
[37] M. Bohner, Calcium orthophosphates in medicine: from ceramics to calcium phosphate cements, Injury 31, Supplement 4(0) (2000) D37-D47.
[38] C. Wang, Y. Duan, B. Markovic, J. Barbara, C.R. Howlett, X. Zhang, H. Zreiqat, Phenotypic expression of bone-related genes in osteoblasts grown on calcium phosphate ceramics with different phase compositions, Biomaterials 25(13) (2004) 2507-2514.
[39] G. Muralithran, S. Ramesh, The effects of sintering temperature on the properties of hydroxyapatite, Ceramics International 26(2) (2000) 221-230.
[40] H.-S. Ryu, H.-J. Youn, K. Sun Hong, B.-S. Chang, C.-K. Lee, S.-S. Chung, An improvement in sintering property of β-tricalcium phosphate by addition of calcium pyrophosphate, Biomaterials 23(3) (2002) 909-914.
[41] M. Peroglio, L. Gremillard, C. Gauthier, L. Chazeau, S. Verrier, M. Alini, J. Chevalier, Mechanical properties and cytocompatibility of poly(ε-caprolactone)-infiltrated biphasic calcium phosphate scaffolds with bimodal pore distribution, Acta Biomaterialia 6(11) (2010) 4369-4379.
[42] L. Tirkkonen, H. Halonen, J. Hyttinen, H. Kuokkanen, H. Sievänen, A.-M. Koivisto, B. Mannerström, G.K.B. Sándor, R. Suuronen, S. Miettinen, S. Haimi, The effects of vibration loading on adipose stem cell number, viability and differentiation towards bone-forming cells, Journal of The Royal Society Interface 8(65) (2011) 1736-1747.
[43] C. Loebel, E.M. Czekanska, M. Bruderer, G. Salzmann, M. Alini, M.J. Stoddart, In Vitro Osteogenic Potential of Human Mesenchymal Stem Cells Is Predicted by Runx2/Sox9 Ratio, Tissue Engineering Part A (2014).
[44] Z.F. Chen, B.W. Darvell, V.W.H. Leung, Hydroxyapatite solubility in simple inorganic solutions, Archives of Oral Biology 49(5) (2004) 359-367.
[45] E.C. Moreno, T. Aoba, Comparative solubility study of human dental enamel, dentin, and hydroxyapatite, Calcif Tissue Int 49(1) (1991) 6-13.
[46] Y. Avnimelech, E. Moreno, W. Brown, Solubility and surface properties of finely divided hydroxyapatite, J Res Nat Bur Stand 77 (1973) 149-55.
[47] G. Bernardi, [29] Chromatography of proteins on hydroxyapatite, Methods in Enzymology, Academic Press1971, pp. 325-339.
[48] Z. Sadeghian, J.G. Heinrich, F. Moztarzadeh, Preparation of highly concentrated aqueous hydroxyapatite suspensions for slip casting, J Mater Sci 40(17) (2005) 4619-4623.
[49] L.C. Bell, A.M. Posner, J.P. Quirk, The point of zero charge of hydroxyapatite and fluorapatite in aqueous solutions, Journal of Colloid and Interface Science 42(2) (1973) 250-261.
[50] I.S. Harding, N. Rashid, K.A. Hing, Surface charge and the effect of excess calcium ions on the hydroxyapatite surface, Biomaterials 26(34) (2005) 6818-6826.
[51] L.M. Rodríguez-Lorenzo, M. Vallet-Regí, J.M.F. Ferreira, Colloidal processing of hydroxyapatite, Biomaterials 22(13) (2001) 1847-1852.
[52] J. Ma, C.H. Liang, L.B. Kong, C. Wang, Colloidal characterization and electrophoretic deposition of hydroxyapatite on titanium substrate, J Mater Sci: Mater Med 14(9) (2003) 797-801.
[53] X. Yao, S. Tan, D. Jiang, Fabrication of hydroxyapatite ceramics with controlled pore characteristics by slip casting, J Mater Sci: Mater Med 16(2) (2005) 161-165.

[54] V. Uskoković, R. Odsinada, S. Djordjevic, S. Habelitz, Dynamic light scattering and zeta potential of colloidal mixtures of amelogenin and hydroxyapatite in calcium and phosphate rich ionic milieus, Archives of Oral Biology 56(6) (2011) 521-532.
[55] M. Mourabet, A. El Rhilassi, H. El Boujaady, M. Bennani-Ziatni, R. El Hamri, A. Taitai, Removal of fluoride from aqueous solution by adsorption on Apatitic tricalcium phosphate using Box–Behnken design and desirability function, Applied Surface Science 258(10) (2012) 4402-4410.
[56] E. Garcia-Tunon, S. Barg, R. Bell, J.V.M. Weaver, C. Walter, L. Goyos, E. Saiz, Designing Smart Particles for the Assembly of Complex Macroscopic Structures, Angewandte Chemie International Edition 52(30) (2013) 7805-7808.
[57] P.N. Sturzenegger, U.T. Gonzenbach, S. Koltzenburg, L.J. Gauckler, Controlling the formation of particle-stabilized water-in-oil emulsions, Soft Matter 8(28) (2012) 7471-7479.
[58] K. Anselme, M. Bigerelle, Role of materials surface topography on mammalian cell response, International Materials Reviews 56(4) (2011) 243-266.
[59] K. Anselme, M. Bigerelle, Topography effects of pure titanium substrates on human osteoblast long-term adhesion, Acta Biomaterialia 1(2) (2005) 211-222.
[60] K. Anselme, Osteoblast adhesion on biomaterials, Biomaterials 21(7) (2000) 667-681.
[61] O. Zinger, K. Anselme, A. Denzer, P. Habersetzer, M. Wieland, J. Jeanfils, P. Hardouin, D. Landolt, Time-dependent morphology and adhesion of osteoblastic cells on titanium model surfaces featuring scale-resolved topography, Biomaterials 25(14) (2004) 2695-2711.
[62] L. Baxter, V. Frauchiger, M. Textor, I. Ap Gwynn, R. Richards, Fibroblast and osteoblast adhesion and morphology on calcium phosphate surfaces, Eur Cell Mater 4 (2002) 1-17.
[63] X. Lu, Y. Leng, Theoretical analysis of calcium phosphate precipitation in simulated body fluid, Biomaterials 26(10) (2005) 1097-1108.
[64] H.-M. Kim, T. Himeno, M. Kawashita, T. Kokubo, T. Nakamura, The mechanism of biomineralization of bone-like apatite on synthetic hydroxyapatite: an in vitro assessment, Journal of The Royal Society Interface 1(1) (2004) 17-22.
[65] J.T.Y. Lee, Y. Leng, K.L. Chow, F. Ren, X. Ge, K. Wang, X. Lu, Cell culture medium as an alternative to conventional simulated body fluid, Acta Biomaterialia 7(6) (2011) 2615-2622.
[66] D.D. Deligianni, N. Katsala, S. Ladas, D. Sotiropoulou, J. Amedee, Y.F. Missirlis, Effect of surface roughness of the titanium alloy Ti–6Al–4V on human bone marrow cell response and on protein adsorption, Biomaterials 22(11) (2001) 1241-1251.
[67] K. Anselme, P. Linez, M. Bigerelle, D. Le Maguer, A. Le Maguer, P. Hardouin, H.F. Hildebrand, A. Iost, J.M. Leroy, The relative influence of the topography and chemistry of TiAl6V4 surfaces on osteoblastic cell behaviour, Biomaterials 21(15) (2000) 1567-1577.
[68] M. Bigerelle, K. Anselme, B. Noël, I. Ruderman, P. Hardouin, A. Iost, Improvement in the morphology of Ti-based surfaces: a new process to increase in vitro human osteoblast response, Biomaterials 23(7) (2002) 1563-1577.
[69] M.J. Dalby, N. Gadegaard, R. Tare, A. Andar, M.O. Riehle, P. Herzyk, C.D. Wilkinson, R.O. Oreffo, The control of human mesenchymal cell differentiation using nanoscale symmetry and disorder, Nature materials 6(12) (2007) 997-1003.
[70] H. Yuan, H. Fernandes, P. Habibovic, J. de Boer, A.M. Barradas, A. de Ruiter, W.R. Walsh, C.A. van Blitterswijk, J.D. de Bruijn, Osteoinductive ceramics as a synthetic alternative to autologous bone grafting, Proceedings of the National Academy of Sciences 107(31) (2010) 13614-13619.

Figure 1 – General overview of the processing steps adopted to fabricate scaffolds with controlled microstructure from high solid content BCS-functionalised calcium phosphate suspensions. Decane (hydrophobic) is added to the ceramic suspension and emulsified into droplets (right). Alternatively, this emulsification step may be skipped, resulting in materials without oil-derived microporosity (left). Glucono-δ-lactone is added to trigger a homogeneous decrease in pH, after which the materials are cast, allowed to dry and sintered. Processing of BCS-functionalised calcium phosphates to prepare: Top) microporous materials resulting from the oil templating (emulsified suspensions); Bottom) concentrated ceramic suspensions with no oil derived porosity

Figure 2 – Effect of BCS and GδL concentration on ceramic suspensions prepared with HA and β-TCP. A, B and C) BCS acts as a dispersant in aqueous suspensions of HA and β-TCP (70 wt%) at basic pH (~8). BCS 2 wt% results in a lower D_{50} than with Dolapix. D) pH variation in aqueous solutions of BCS 2 wt% after addition of different amounts of GδL (0,1 to 4 wt%). E) pH evolution of ceramic suspensions (HA and β-TCP) and emulsions prepared with BCS 2 wt% and different solid content (45, 60 or 70 wt%)

Figure 3 – A, B and C) Fluorescence microscopy images of emulsified HA 10 vol% functionalised with BCSr 2 wt%. A) Series of images of a single location at different depths of focus; B) Arrows show fluorescent particle-BCSr agglomerates at the oil droplet/ceramic suspension interface across the oil droplet; C) Arrows show increased fluorescence at the oil droplet/ceramic suspension interface; D) SEM images of porous HA and β-TCP scaffolds after emulsification with 50 vol% decane, aggregation with 1 wt/v% GδL, drying and sintering. (top) 70 wt% green bodies; (middle) 70 wt% sintered; (bottom) 60 wt% sintered

Figure 4 – A) SEM images of porous 70 wt% HA (left) and β-TCP (right) scaffolds emulsified at different speeds: manual agitation (MA), MA + 1 min at 24000 rpm, MA + 2.5 min at 24000 rpm, MA + 10 min at 24000 rpm; B) Pore diameter of HA, β-TCP and biphasic calcium phosphate microporous materials decreases with increasing emulsification energy; C) Compressive strength of materials with varying composition (HA, biphasic compositions and β-TCP) decreases with emulsification energy; D) SEM image of 70 wt% HA sample prepared without oil ("no oil")

Figure 5 – A) Surface maps (left) and surface line profiles (right) of β-TCP discs. (Top) No oil; (middle) 1 min emulsification; (bottom) 2.5 min emulsification. Colour map indicates depth of the features: red represents peaks, blue represents pits. Area: 290x220 μm^2; B) R_a of the three surface types: No oil, 2.5 min and 1 min). $p < 0.001$ (***) and $p < 0.0001$ (****); C and D) SEM images of biphasic porous constructs prepared with 50/50 HA/β-TCP wt% and two different emulsification times (1 and 2.5 min)

Figure 6 – A) Representative SEM images of human mesenchymal stem cells cultured on calcium phosphate substrates with different surface properties (No oil, 1 min and 2.5 min) for 48h; B) cell area and C) cell perimeter of hMSCs cultured on ceramic substrates for 2 and 48 hours. Data are presented as mean ± standard error of mean (n>10). Significant differences are reported when $p<0.01$ (**), $p<0.001$ (***) and $p<0.0001$ (****). * refers to the same group at different time points. # refers to different chemical compositions, but same surface type

Figure 7 – SEM images of calcium phosphate substrates cultured with hMSCs in osteogenic DMEM for 2 and 7 days, showing surface microstructure does not change in that period. A and B) HA 1 min samples incubated for 2 and 7 days, respectively. C and D) β-TCP No oil samples incubated for 2 and 7 days, respectively

Figure 8 – A) Cell attachment (24h after cell seeding) and B) cell proliferation up to day 28. Data are presented as mean ± standard error of mean (n=3). Significant differences are reported when $p<0.05$ (*), $p<0.01$ (**), $p<0.001$ (***) and $p<0.0001$ (****). a ($p<0.05$), b ($p<0.01$), c ($p<0.001$) and d ($p<0.0001$) refer to differences between Control and ceramic substrate at the same time point. * refers to the same group at different time points. # refers to different chemical compositions, but same surface type

Figure 9 - A) ALP activity of hMSCs on HA, BCP and β-TCP substrates. Data are presented as mean ± standard error of mean (n=3). Significant differences are reported when $p<0.05$ (*), $p<0.01$ (**), $p<0.001$ (***) and $p<0.0001$ (****). a ($p<0.05$), b ($p<0.01$), c ($p<0.001$) and d ($p<0.0001$) refer to differences between Control and ceramic substrate at the same time point. * refers to the same group at different time points. # refers to different chemical compositions, but same surface type. B) ALP staining of hMSCs. Control is a Thermanox® slide. Scale bar = 5mm

Figure 10 – Representative gene expression profile of hMSCs cultured for 28 days on ceramic substrates: A) type I collagen (Col1), B) alkaline phosphatase (ALP), C) osteocalcin (OC). mRNA levels are expressed relative to 18S endogenous control and normalised to cells at Day 0. Data are presented as mean ± standard error of mean (n=3). Significant differences are reported when $p<0.05$ (*), $p<0.01$ (**), $p<0.001$ (***) and $p<0.0001$ (****). a ($p<0.05$), b ($p<0.01$), c ($p<0.001$) and d ($p<0.0001$) refer to differences between Control and ceramic substrate at the same time point. * refers to the same group at different time points. # refers to different chemical compositions, but same surface type

Figure 11 – Representative gene expression profile of hMSCs cultured for 28 days on ceramic substrates: A) runx-related transcription factor 2 (Runx2), B) sex determining region Y-box (Sox9), C) Runx2/Sox9 ratio. mRNA levels are expressed relative to 18S endogenous control and normalised to cells at Day 0. Data are presented as mean ± standard error of mean (n=3). Significant differences are reported when $p<0.05$ (*), $p<0.01$ (**), $p<0.001$ (***) and $p<0.0001$ (****). a ($p<0.05$), b ($p<0.01$), c ($p<0.001$) and d ($p<0.0001$) refer to differences between Control and ceramic substrate at the same time point. * refers to the same group at different time points. # refers to different chemical compositions, but same surface type

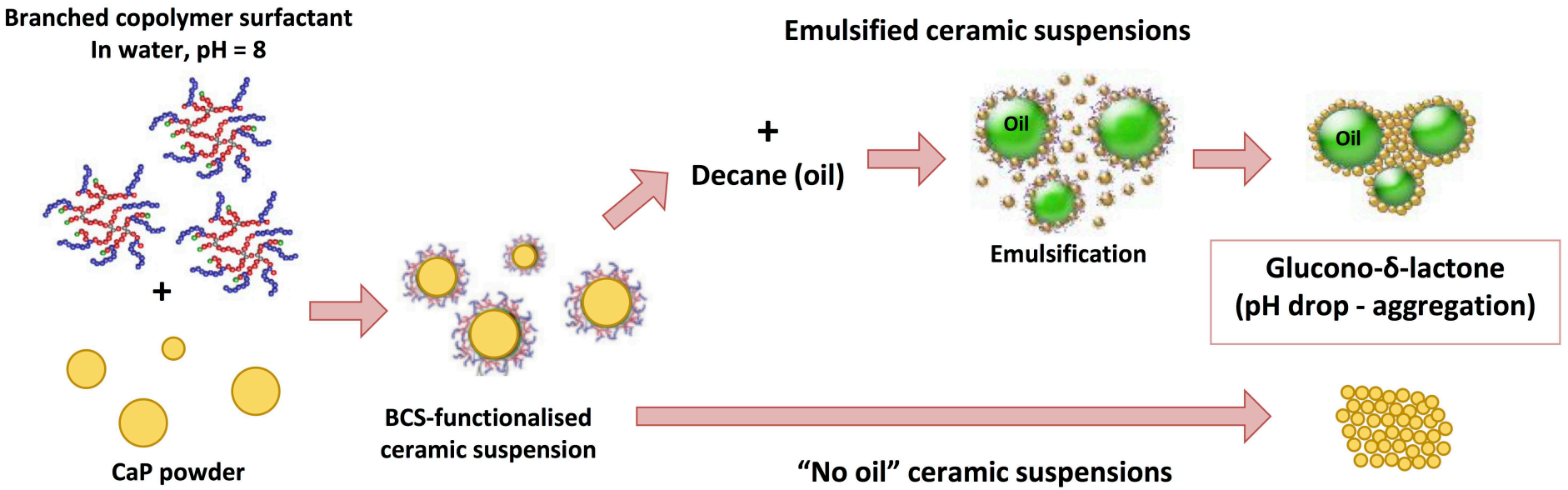
Branched copolymer surfactant
In water, pH = 8
+
CaP powder
BCS-functionalised
ceramic suspension
+
Decane (oil)
Emulsified ceramic suspensions
Oil
Emulsification
Oil
Glucono-δ-lactone
(pH drop - aggregation)
"No oil" ceramic suspensions

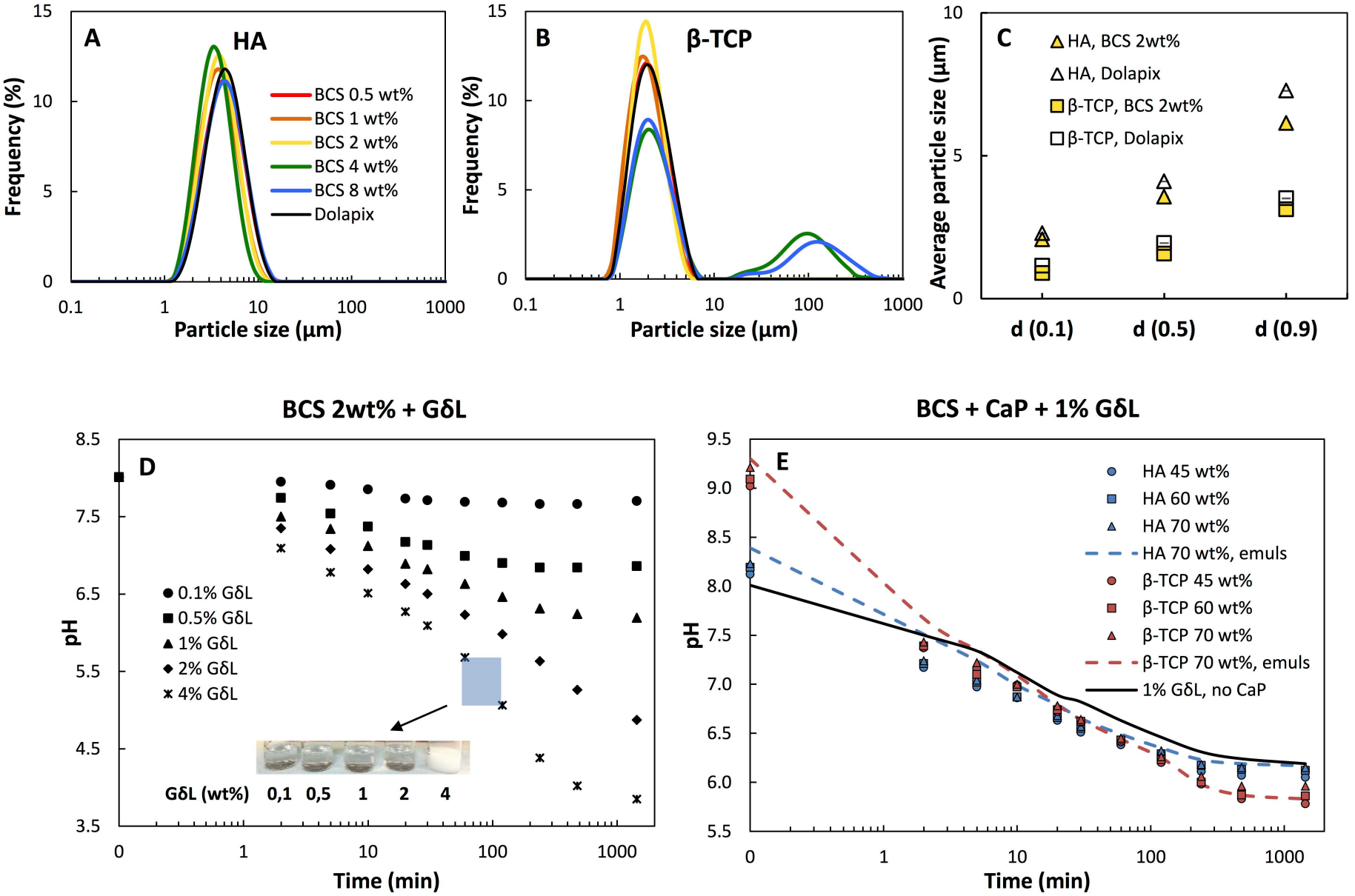
A
HA
BCS 0.5 wt%
BCS 1 wt%
BCS 2 wt%
BCS 4 wt%
BCS 8 wt%
Dolapix
Frequency (%)
Particle size (µm)
B
β-TCP
Frequency (%)
Particle size (µm)
C
HA, BCS 2wt%
HA, Dolapix
β-TCP, BCS 2wt%
β-TCP, Dolapix
Average particle size (µm)
d (0.1)
d (0.5)
d (0.9)
BCS 2wt% + GδL
D
0.1% GδL
0.5% GδL
1% GδL
2% GδL
4% GδL
GδL (wt%) 0,1 0,5 1 2 4
pH
Time (min)
BCS + CaP + 1% GδL
E
HA 45 wt%
HA 60 wt%
HA 70 wt%
HA 70 wt%, emuls
β-TCP 45 wt%
β-TCP 60 wt%
β-TCP 70 wt%
β-TCP 70 wt%, emuls
1% GδL, no CaP
pH
Time (min)

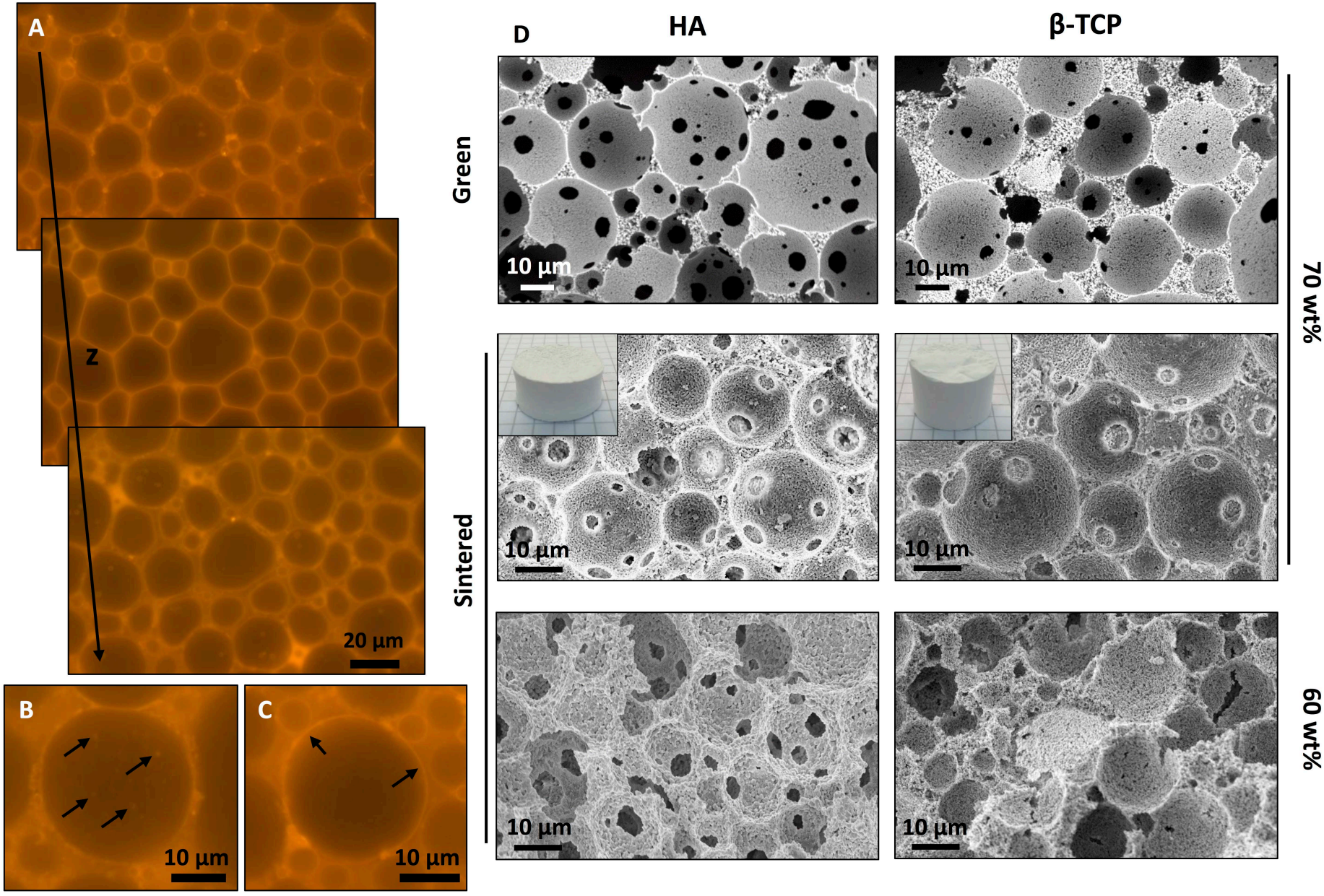
A
Z
20 µm
B
10 µm
C
10 µm
D
HA
β-TCP
Green
Sintered
10 µm
10 µm
10 µm
10 µm
10 µm
10 µm
70 wt%
60 wt%

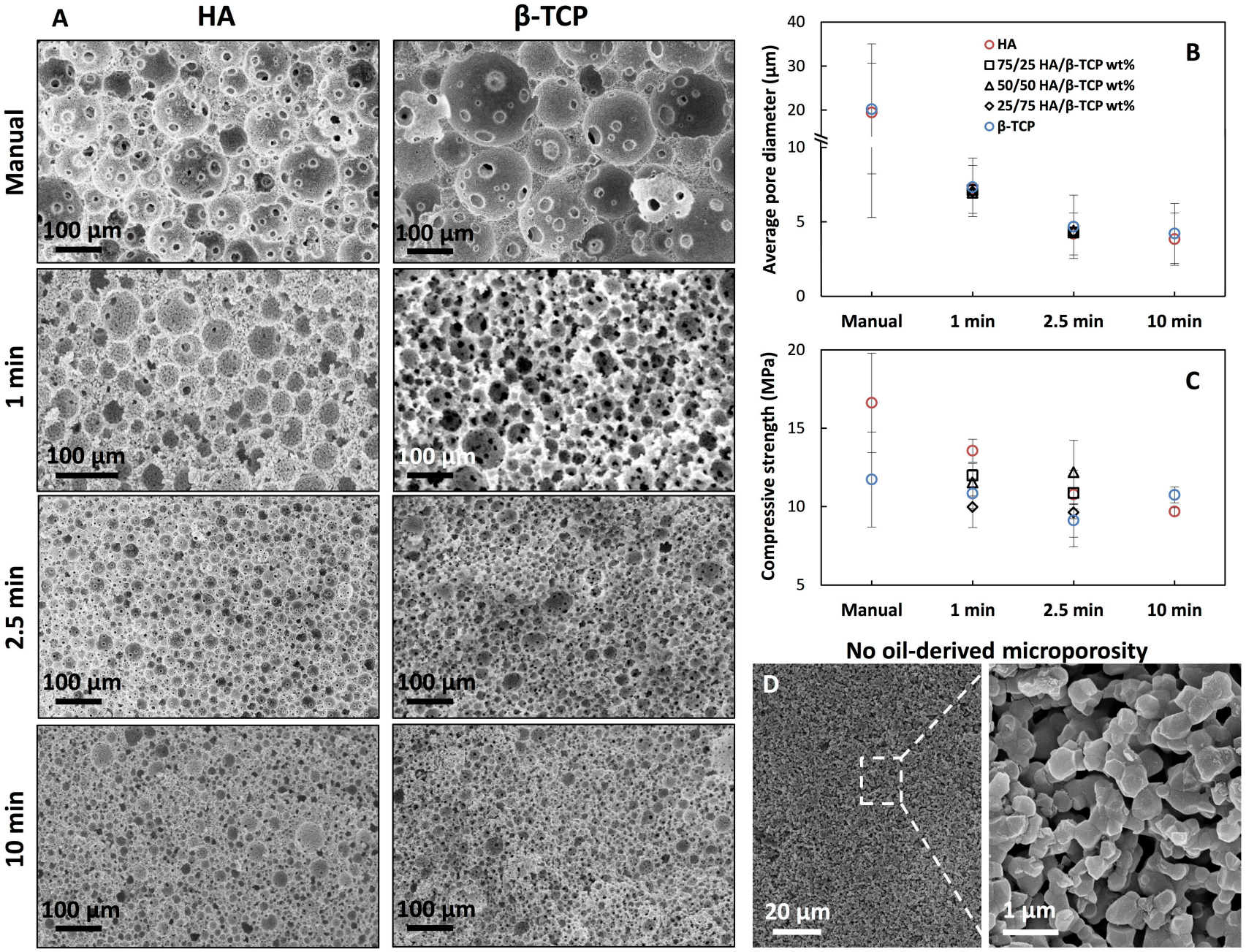
A
HA
β-TCP
Manual
1 min
2.5 min
10 min
100 µm
B
Average pore diameter (µm)
HA
75/25 HA/β-TCP wt%
50/50 HA/β-TCP wt%
25/75 HA/β-TCP wt%
β-TCP
Manual
1 min
2.5 min
10 min
C
Compressive strength (MPa)
No oil-derived microporosity
D
20 µm
1 µm

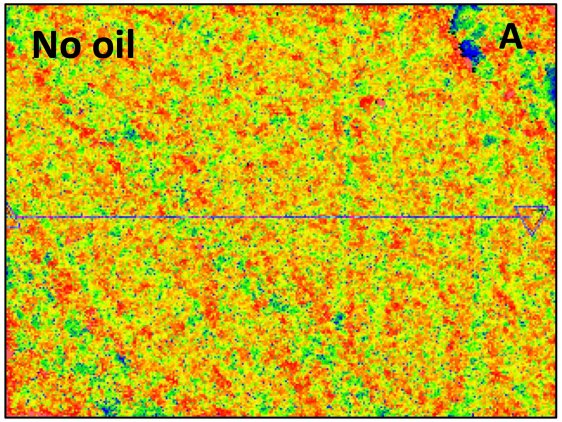

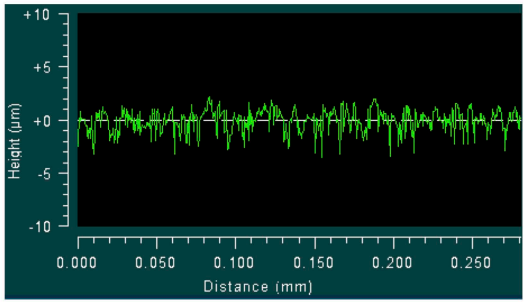

+ 46,810 µm

- 47,235 µm

R_a = 0.923 ± 0.064 µm

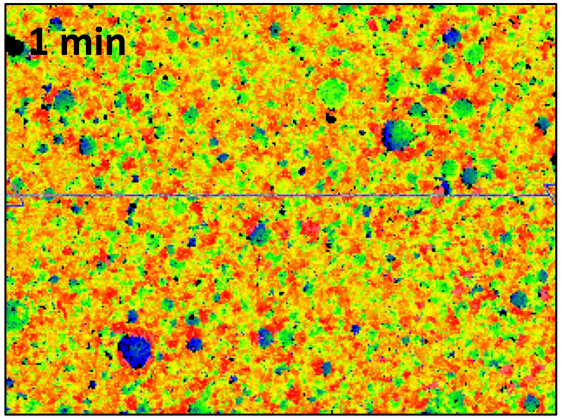

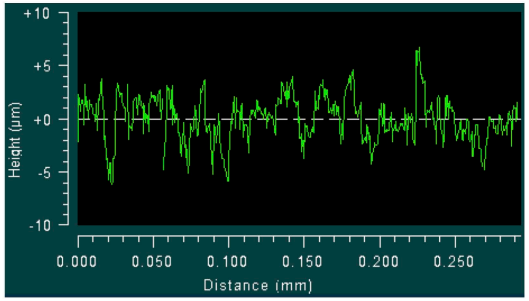

+ 47,203 µm

- 50,982 µm

R_a = 1.691 ± 0.071 µm

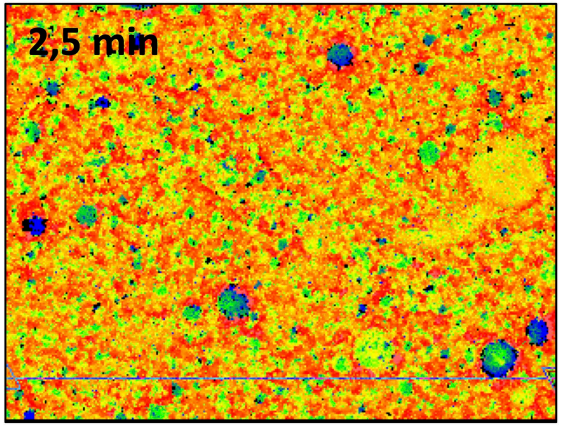

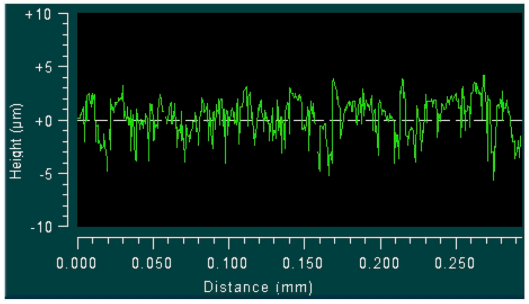

+ 49,019 µm

- 50,027 µm

R_a = 1.475 ± 0.035 µm

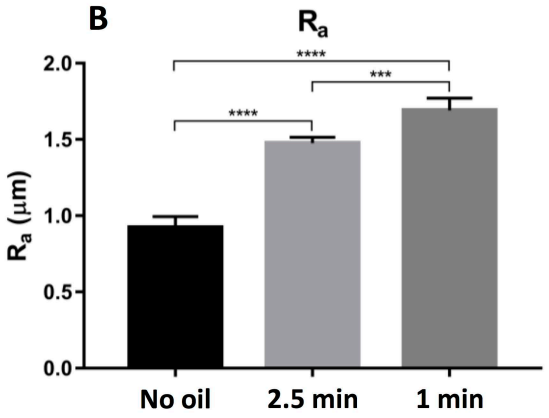

HA/β-TCP 50/50 wt%

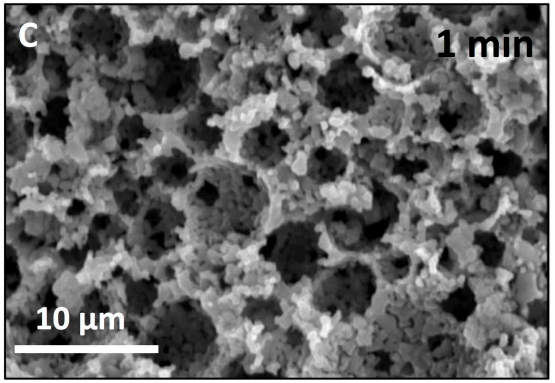

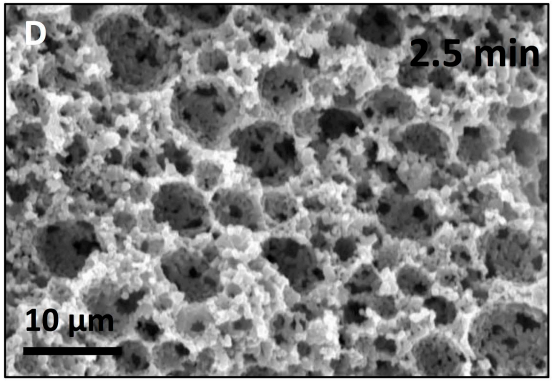

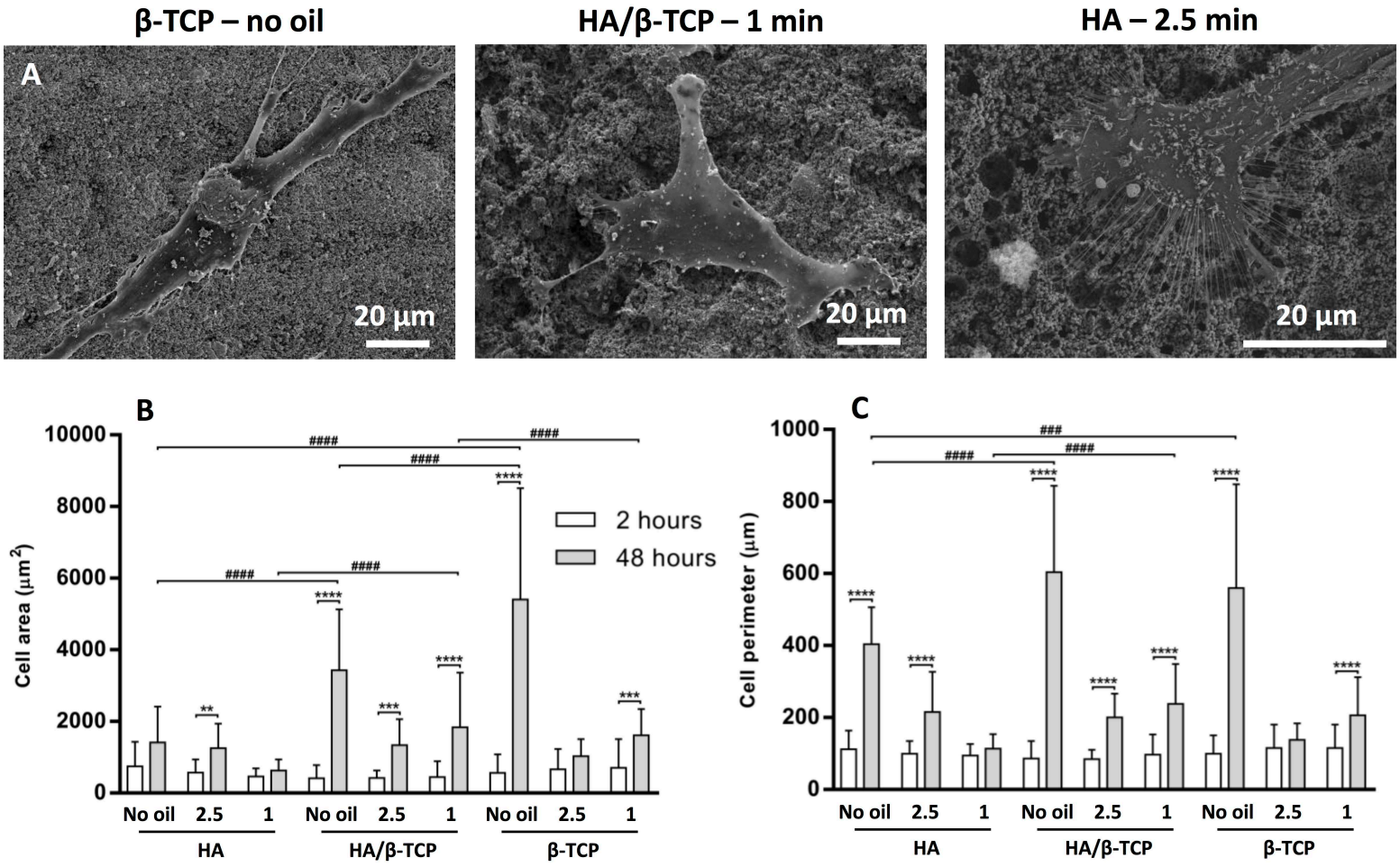
β-TCP – no oil
HA/β-TCP – 1 min
HA – 2.5 min
A
20 µm
20 µm
20 µm
B
Cell area (µm²)
10000
8000
6000
4000
2000
0
2 hours
48 hours
No oil
2.5
1
HA
HA/β-TCP
β-TCP
C
Cell perimeter (µm)
1000
800
600
400
200
0

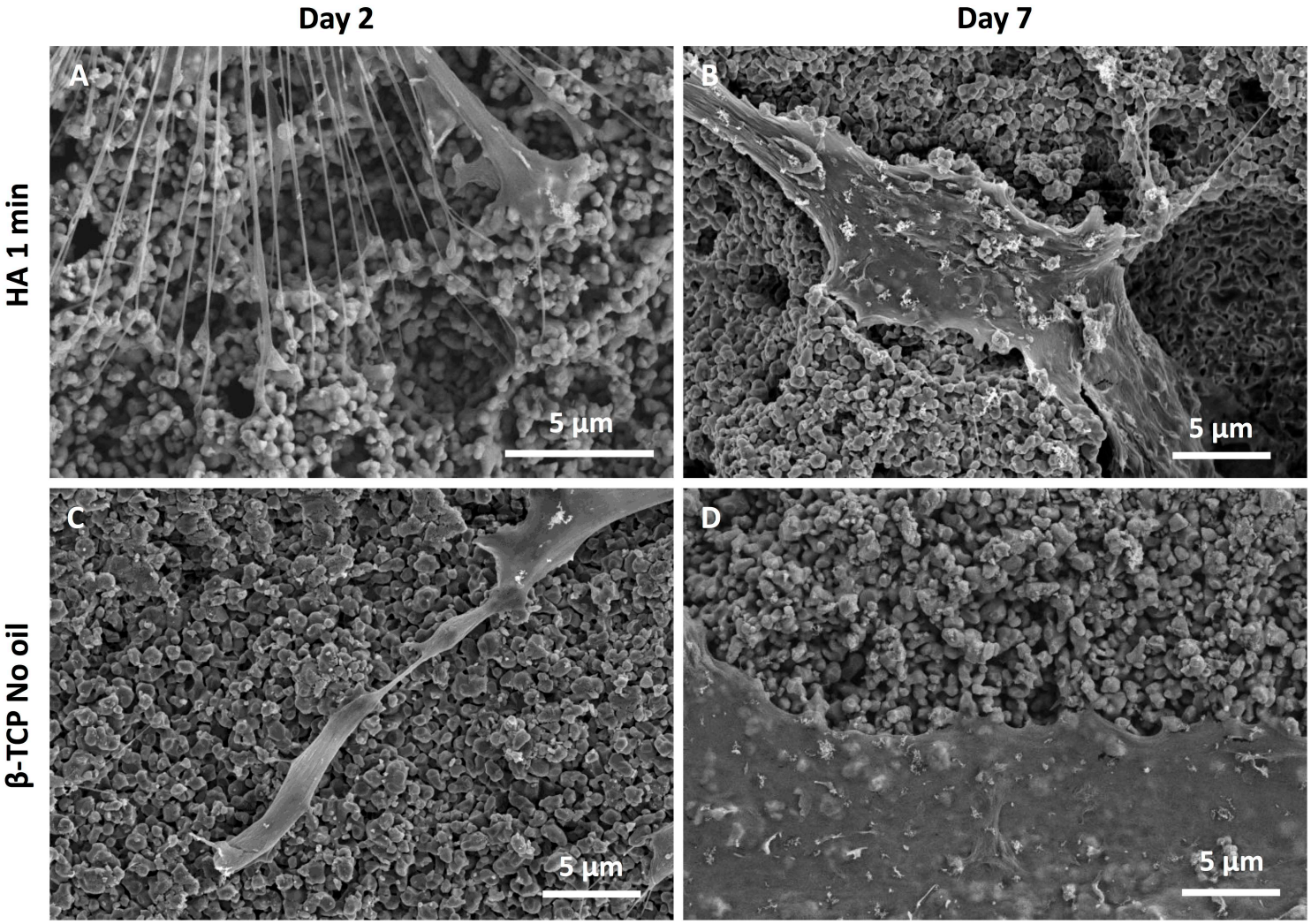
Day 2
Day 7
HA 1 min
β-TCP No oil
A
B
C
D
5 µm
5 µm
5 µm
5 µm

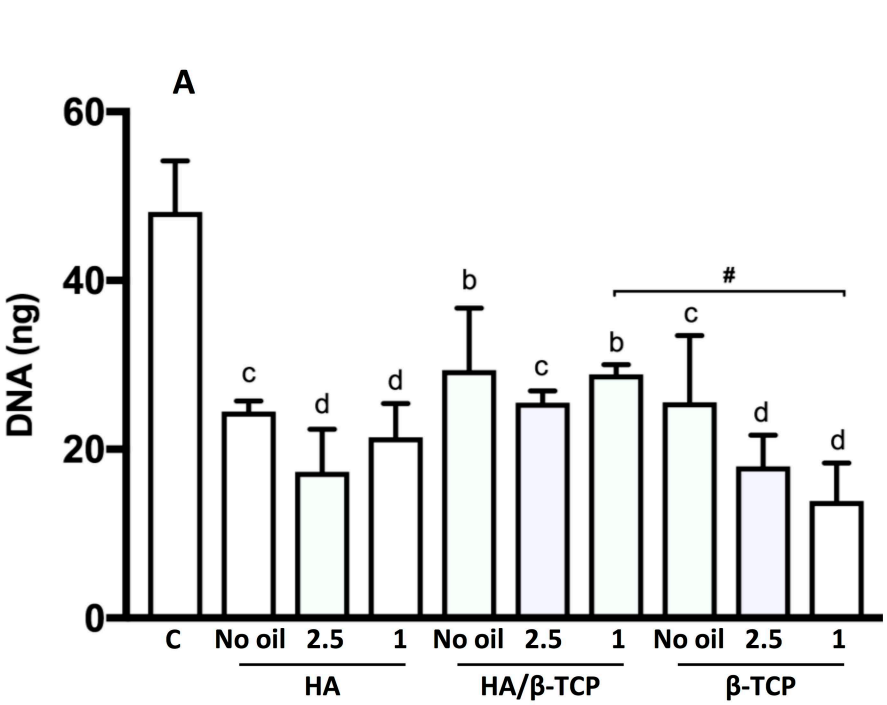
A
DNA (ng)
60
40
20
0
c
d
d
b
c
b
c
d
d
#
C
No oil
2.5
1
No oil
2.5
1
No oil
2.5
1
HA
HA/β-TCP
β-TCP

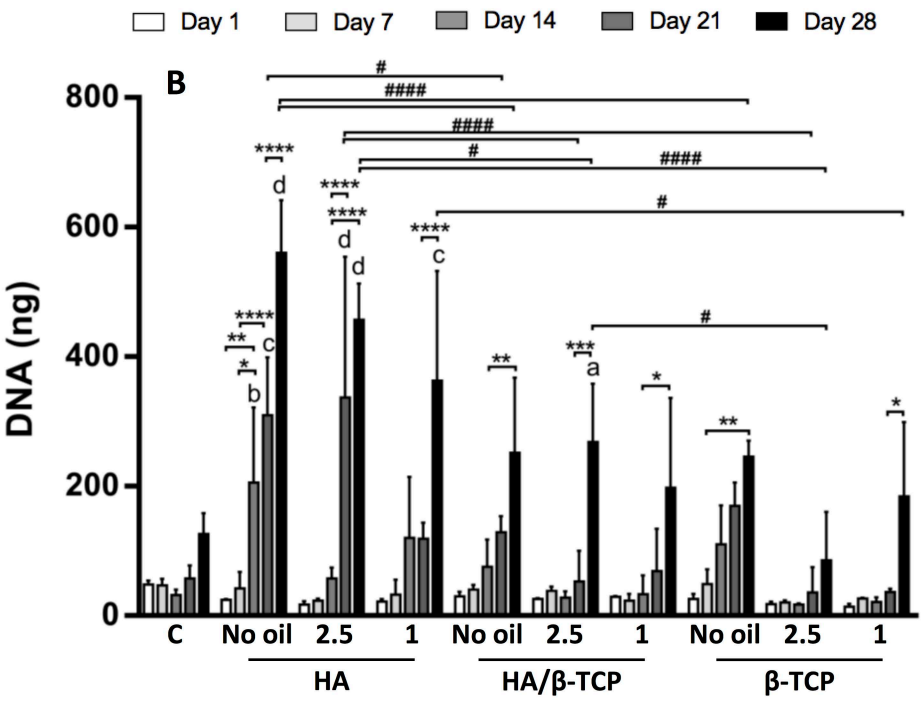
Day 1
Day 7
Day 14
Day 21
Day 28
B
DNA (ng)
800
600
400
200
0
#
####
####
#
####
#
#
****
****
****
****
**
*
****
***
**
*
**
*
C
No oil
2.5
1
No oil
2.5
1
No oil
2.5
1
HA
HA/β-TCP
β-TCP

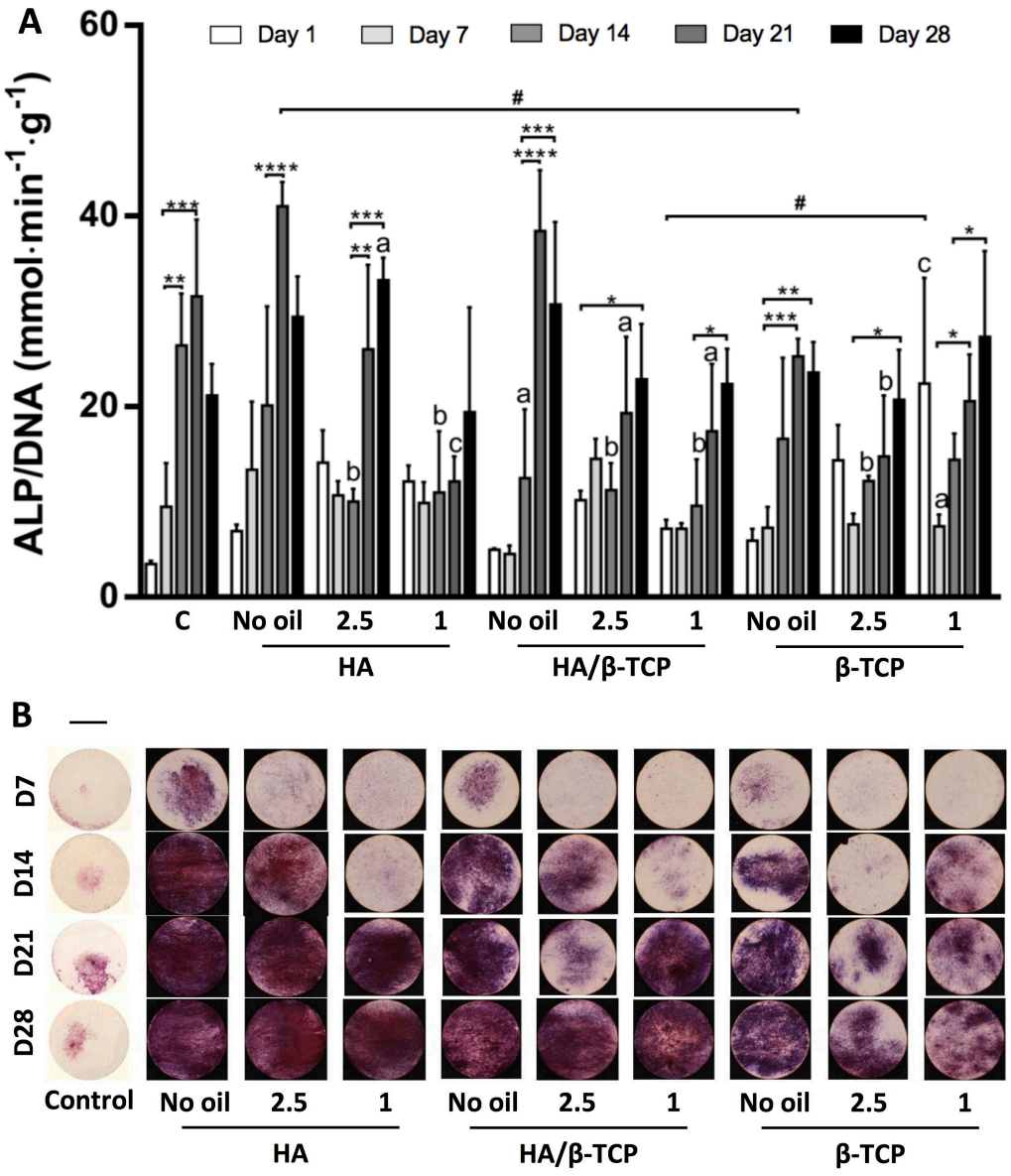
A
Day 1
Day 7
Day 14
Day 21
Day 28
ALP/DNA (mmol·min-1.g-1)
60
40
20
0
C
No oil
2.5
1
HA
HA/β-TCP
β-TCP
B
D7
D14
D21
D28
Control

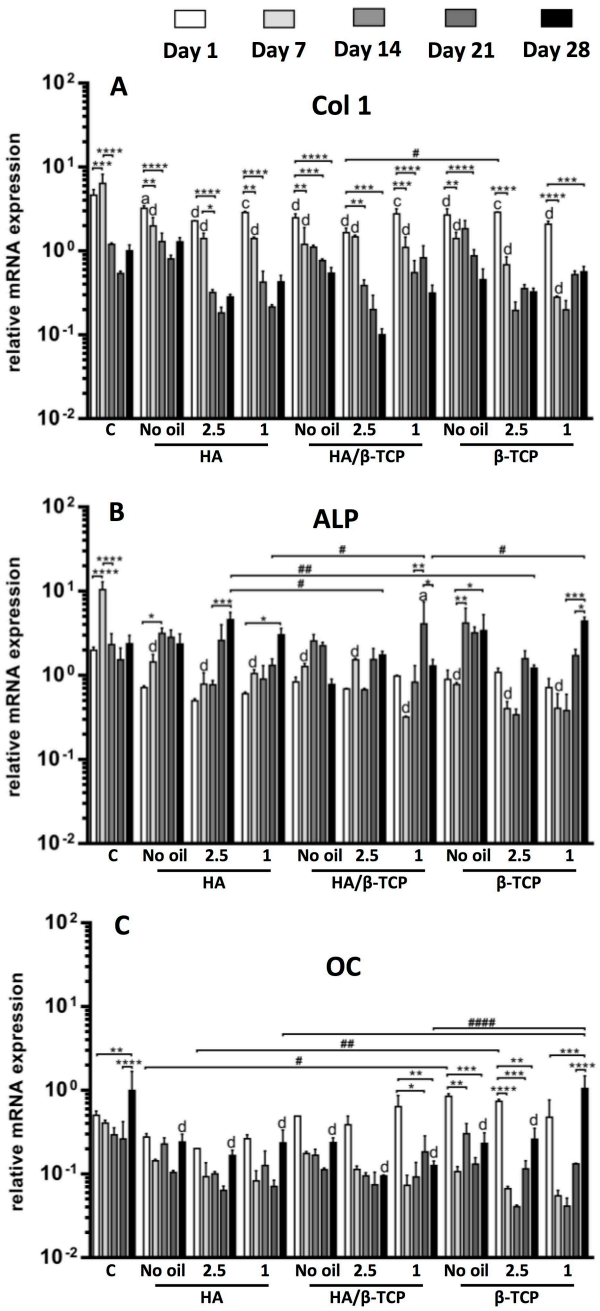
Day 1
Day 7
Day 14
Day 21
Day 28
A
Col 1
B
ALP
C
OC
relative mRNA expression
C
No oil
2.5
1
HA
HA/β-TCP
β-TCP

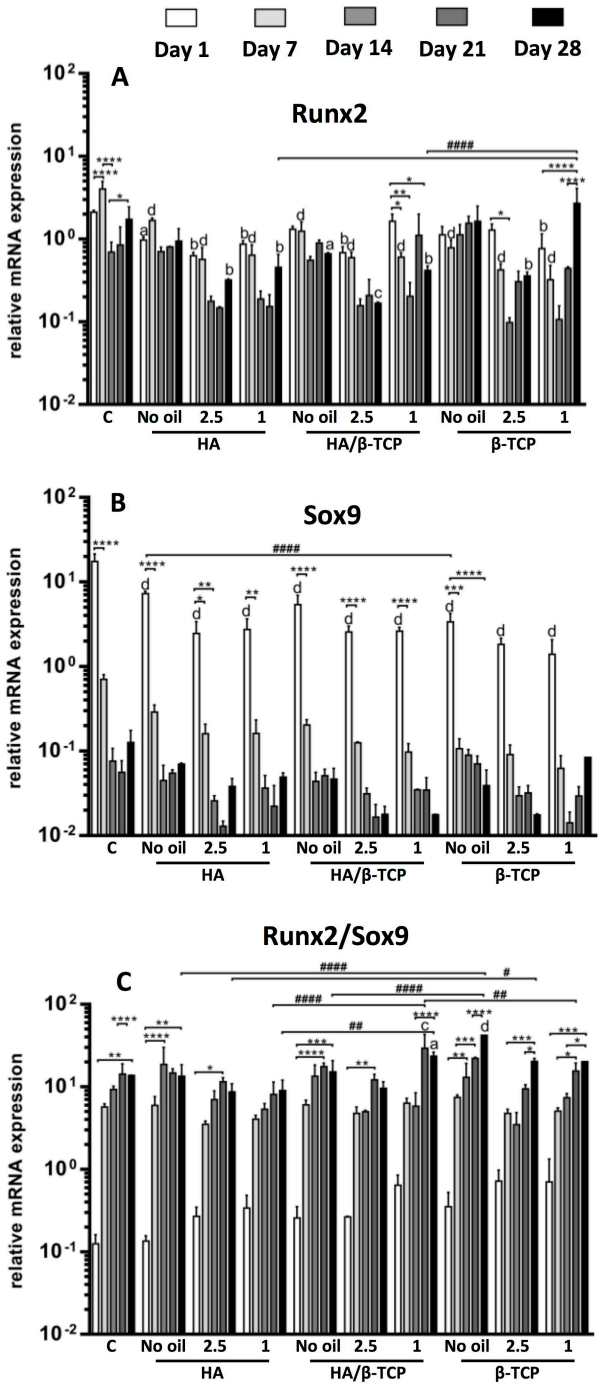
Day 1
Day 7
Day 14
Day 21
Day 28
A
Runx2
relative mRNA expression
C
No oil
2.5
1
HA
HA/β-TCP
β-TCP
B
Sox9
Runx2/Sox9
C

Table 1 - Forward (fw), reverse (rv) primers and probe sequences for type I collagen (COL1), runx2 and osteocalcin (OC) gene expression analysis were purchased from Microsynth (Switzerland). Alkaline phosphatase (ALP), Sox9 and 18s gene assays were from Applied Biosystems (USA)

18S	Hs99999901_s1
ALP	Hs00758162_m1
Sox9	Hs00165814_m1
COL1	**Fw** 5'-CCC TGG AAA GAA TGG AGA TGA T-3' **Rv** 5'-ACT GAA ACC TCT GTG TCC CTT CA-3' **Probe** 5'-CGG GCA ATC CTC GAG CAC CCT -3'
Runx2	**Fw** 5'-AGC AAG GTT CAA CGA TCT GAG AT-3' **Rv** 5'-TTT GTG AAG ACG GTT ATG GTC AA-3' **Probe** 5'-TGA AAC TCT TGC CTC GTC CAC TCC G-3'
OC	**Fw** 5'-AAG AGA CCC AGG CGC TAC CT-3' **Rv** 5'-AAC TCG TCA CAG TCC GGA TTG-3' **Probe** 5'-ATG GCT GGG AGC CCC AGT CCC-3'